

Tensor Rules in the Stochastic Organization of Genomes and Genetic Stochastic Resonance in Algebraic Biology

Sergey V. Petoukhov

Mechanical Engineering Research Institute of Russian Academy of Sciences. Russia, 101990, Moscow, M.
Kharitonievskiy pereulok, 4,
<http://eng.imash.ru/>, info@imash.ru

Comment: Some materials of this article were presented by the author in his keynote speech at the International Symmetry Festival-2021 (Sophia, Bulgaria, 9-12 July 2021, <https://festival.symmetry.hu/>) and in his speech at the Seventh International Conference in Code Biology (Lužnica, Croatia, 31 August – 4 September 2021, <https://www.codebiology.org/conferences/Luznica2021/>).

Abstract. The article is devoted to the new results of the author, which add his previously published ones, of studying hidden rules and symmetries in structures of long single-stranded DNA sequences in eukaryotic and prokaryotic genomes. The author uses the existence of different alphabets of n-plets in DNA: the alphabet of 4 nucleotides, the alphabet of 16 douplets, the alphabet of 64 triplets, etc. Each of such DNA alphabets of n-plets can serve for constructing a text as a chain of these n-plets. Using this possibility, the author represents any long DNA nucleotide sequence as a bunch of many so-called n-texts, each of which is written on the basis of one of these alphabets of n-plets. Each of such n-texts has its individual percents of different n-plets in its genomic DNA. But it turns out that in such multi-alphabetical or multilayer presentation of each of many genomic DNA, analyzed by the author, universal rules of probabilities and symmetry exist in interrelations of its different n-texts regarding their percents of n-plets. In this study, the tensor product of matrices and vectors is used as an effective analytical tool borrowed from the arsenal of quantum mechanics. Some additions to the topic of algebra-holographic principles in genetics are also presented. Taking into account the described genomic rules of probability, the author puts also forward a concept of the important role of stochastic resonances in genetic informatics.

Keywords: genome, DNA, alphabet, matrices, tensor product, quantum informatics, stochastic resonance.

Content

1. Introduction.
2. Tensor interrelations of the percentage of oligomers in n-texts of the genomic DNA.
3. Regarding the connection of the stochastic phenomenon of tetra-colonies of n-plets in genomic n-texts with quantum formalisms of vectors of probability amplitudes.
4. Equality of the sums of probabilities of n-plets in binary-inversinable pairs of rows and columns of genomic probability matrices.
5. Symmetry of percentages of mirror-complemented n-plets in n-texts of genomic DNA.
6. Some additions to algebra-holographic principles in the genetic system.
7. Rademacher functions and universal rules of probabilities in n-texts of genomic DNA.
8. Genetic stochastic resonance in algebraic biology.
 - 8.1. Introduction data about stochastic resonance.
 - 8.2. Stochastic resonance in genetically inherited physiological systems.
 - 8.3. Genetic stochastic resonance.
 - 8.4. Genetic stochastic resonance and inherited human affinity with music.
9. Some concluding remarks.
 - Appendix I. Regarding the tensor product of matrices.
 - Acknowledgments
 - References

1. Introduction.

This article continues a description of the author's results, which add his previously published ones, of studying universal rules and symmetries in structures of long single-stranded DNA sequences in eukaryotic and prokaryotic genomes.

Genetic DNA molecules belong to the microworld, in which the principles of quantum mechanics reign. Quantum mechanics is a probabilistic theory. No wonder one of the founders of quantum mechanics and the author of the first article on quantum biology P. Jordan claimed that that life's missing laws are the rules of chance and probability of the quantum world that were somehow scaled up inside living organisms [Jordan, 1932; McFadden, Al-Khalili, 2018]. For this reason, in this and a number of other works, the author studies the laws of probabilities in long DNA molecules from different genomes.

In his previous articles [Petoukhov, 2021a,b], the author presented algebraic tables of numerical data for universal probability rules of nucleotide sequences of single-stranded DNA in eukaryotic and prokaryotic genomes. Genomic DNA sequences are very long: for example, the DNA of human chromosome №1 contains about 250 million nucleotides A, T, C, and G in a complex stochastic order whose hidden rules are a challenge for modern science.

The mentioned rules are connected with n -plets alphabets of DNA whose nucleotide sequences can be considered as bunches of many parallel texts written in interconnected n -plets alphabets (n -plets are synonyms of oligomers containing n nucleotides). The rules draw attention to genomic phenomena of special tetragroupings (or tetra-colonies) of n -plets and new genomic symmetries. In particular, they give a generalization of the second Chargaff's rule. The rules show the existence of long-range coherence in genomic DNA sequences and reveal new connections of structural features of genomic sequences with formalisms of quantum mechanics and quantum informatics.

These rules were discovered due to an effective author's approach for consideration of long single-stranded DNA nucleotide sequences from points of view of different DNA alphabets. As it is known, there are DNA alphabets of 4 nucleotides, 16 doublets, 64 triplets, etc. Each such alphabet consists of 4^n n -plets (that is, oligomers of fixed length n). Correspondingly, each DNA sequence can be considered not as a separate information text but as a set (or bunch) of many DNA-texts, each of which is written in one of these n -plets alphabets (in other words, in this approach, any DNA sequence is presented as a bunch of messages in different but interrelated "languages"). For example, the DNA sequence ACCTGTAACG... is a bunch of the following texts, which we briefly term as n -texts of the DNA:

- a text of nucleotides (A-C-C-C-T-G- ...) from the point of view of the 1-plet alphabet (it is the 1-text of the DNA);
- a text of doublets (AC-CT-GT-AA-CG- ...) from the point of view of the 2-plet alphabet (it is the 2-text of the DNA);
- a text of triplets (ACC- TGT-AAC- ..) from the point of view of the 3-plet alphabet (it is the 3-text of the DNA);
- and so on for other DNA n -texts under $n = 4, 5, 6, \dots$

In each of such different n -texts of the same long DNA sequence, one can calculate the percentages of each of the 4^n members of the corresponding n -plets alphabet and then compare sets of calculated percentages from different n -texts. This comparative analysis of a wide set of eukaryotic and prokaryotic genomes revealed hidden algebraic interrelations among percentage compositions of these genomic n -texts and allowed formulating fundamental rules of stochastic tetra-colonial organizations of the genomes [Petoukhov, 2020c, 2021a-c]. The revealed rules give pieces of evidence of the existence of global-genomic algebraic invariants, which remain unchanged over millions of years of biological evolution, during which millions of species of organisms die and new ones arise (although locally genomic sequences are modified under the action of mutations, the pressing of natural selection, etc.). Further extensive studies of genomes are required to test the universality of the found rules of probabilities in genomes.

The aim of this article is a continuation of comparative analysis of phenomenologic sets of percentage composition of the different n -texts representing genomic single-stranded DNA sequences from the point of view of the different n -plets alphabets. This continuation has some new results and new forms of presentations of the universal genomic rules of probabilities, and also new data about their structural connections with mathematical formalisms of quantum mechanics and quantum informatics. Special attention will be paid to

the connection between the structural features of multicomponent genetic systems and the tensor product of vectors and matrices since it plays a particularly important role in quantum mechanics and quantum informatics. This connection opens up opportunities for further convergence of genetic informatics with quantum mechanics and quantum informatics taking into account the following.

The tensor product gives a way of putting separate vector spaces together to form larger vector spaces and it is one of the basic instruments in quantum informatics. The following statement illustrates the role of the tensor product: “*This construction is crucial to understanding the quantum mechanics of multiparticle systems*” [Nielsen, Chuang, 2010, p. 71]. It is in line with the postulate of quantum mechanics: the state space of a composite system is the tensor product of the state spaces of its components. More details about the tensor product of matrices can be found in Appendix I.

The described results allow putting forward a hypothesis about a quantum-informational stochastic memory in living bodies on the basis of different n-texts for modeling interconnected stages of ontogenesis: in this model approach, a genomic (n+1)-text represents a later (in comparison to a genomic n-text) stage of ontogenesis associated with the genetic coding of the parametric growth of the developing organism. The reason for this hypothesis was the following phenomenological fact of the stochastic organization of the interconnected n-texts inside any genome: in each genome, the (n+1)-text contains - in its named tetra-colonies of probabilities - information about the tetra-colonies of probabilities inside its n-text. In this model approach, later stages of ontogenesis use genomic n-texts with a higher value n (the interrelations between different n-texts reflect the interrelations between different stages of genetically encoded ontogenesis).

To present new data, the author uses below some data from previous articles [Petoukhov, 2021a-c]. First of all, this is matrices of percentages of n-plets in different n-plets texts of DNA of the human chromosome №1 (Figs. 1.1-1.4) where the symbolic matrices present DNA-alphabets of n-plets in strict orders and are members of a tensor family of matrices $[C, A; T, G]^{(n)}$ (here (n) refers to tensor power n). Percents are shown in fractions of one, and their values are rounded to the fourth decimal place. Initial data on the chromosome were taken in the GenBank: https://www.ncbi.nlm.nih.gov/nuccore/NC_000001.11.

$$\begin{array}{|c|c|c|} \hline & 1 & 0 \\ \hline 1 & C & A \\ \hline 0 & T & G \\ \hline \end{array} \rightarrow \begin{array}{|c|c|c|} \hline & 1 & 0 \\ \hline 1 & \%C & \%A \\ \hline 0 & \%T & \%G \\ \hline \end{array} = \begin{array}{|c|c|c|} \hline & 1 & 0 \\ \hline 1 & 0.2085 & 0.2910 \\ \hline 0 & 0.2918 & 0.2087 \\ \hline \end{array}$$

Fig. 1.1. The matrix of phenomenological percents of each of the 4 nucleotides in the DNA-sequence of nucleotides in the human chromosome №1 (from [Petoukhov, 2021a,b]).

At the first step of the described approach, the DNA-text of the analyzed chromosome is represented as a text of monoplets (for example, the text TAACCCTA... is represented as T-A-A-C-C-C-T-A-...) and percents of each of 4 nucleotides in it are calculated (Fig. 1.1).

At the second step of the described approach, the DNA sequence of the analyzed chromosome is represented as a text of doublets (for example, the text TAACCCTA... is represented as TA-AC-CC-TA-...) and percents of each of 16 doublets are calculated. Then these percents are indicated in appropriate cells of the $(4*4)$ -matrix $[C, A; T, G]^{(2)}$ shown in Fig. 1.2.

$$\begin{array}{|c|c|c|c|c|} \hline & 11 & 10 & 01 & 00 \\ \hline 11 & \%CC & \%CA & \%AC & \%AA \\ \hline 10 & \%CT & \%CG & \%AT & \%AG \\ \hline 01 & \%TC & \%TA & \%GC & \%GA \\ \hline 00 & \%TT & \%TG & \%GT & \%GG \\ \hline \end{array} = \begin{array}{|c|c|c|c|c|} \hline & 11 & 10 & 01 & 00 \\ \hline 11 & 0.05409 & 0.07274 & 0.05033 & 0.09504 \\ \hline 10 & 0.07134 & 0.01031 & 0.07429 & 0.07137 \\ \hline 01 & 0.06008 & 0.06312 & 0.04402 & 0.06008 \\ \hline 00 & 0.09568 & 0.07286 & 0.05046 & 0.05419 \\ \hline \end{array}$$

Fig. 1.2. The matrix of phenomenological percents of each of the 16 doublets in the DNA-sequence of doublets in the human chromosome №1 (from [Petoukhov, 2021a,b]).

The resulting matrix of percentages of 64 triplets in the case, when the DNA sequence of the analyzed chromosome is represented as a text of triplets (like as TAA-CCC-...), is presented in Fig. 1.3.

	111	110	101	100	011	010	001	000
111	%CCC	%CCA	%CAC	%CAA	%ACC	%ACA	%AAC	%AAA
110	%CCT	%CCG	%CAT	%CAG	%ACT	%ACG	%AAT	%AAG
101	%CTC	%CTA	%CGC	%CGA	%ATC	%ATA	%AGC	%AGA
100	%CTT	%CTG	%CGT	%CGG	%ATT	%ATG	%AGT	%AGG
011	%TCC	%TCA	%TAC	%TAA	%GCC	%GCA	%GAC	%GAA
010	%TCT	%TCG	%TAT	%TAG	%GCT	%GCG	%GAT	%GAG
001	%TTC	%TTA	%TGC	%TGA	%GTC	%GTA	%GGC	%GGA
000	%TTT	%TTG	%TGT	%TGG	%GTT	%GTG	%GGT	%GGG

	111	110	101	100	011	010	001	000
111	0.01385	0.01878	0.01524	0.01861	0.01183	0.01977	0.01447	0.03693
110	0.01853	0.00291	0.01789	0.02104	0.01622	0.00254	0.02375	0.01988
101	0.01758	0.01275	0.00251	0.00227	0.01317	0.01942	0.01441	0.02237
100	0.02009	0.02088	0.00259	0.00291	0.02388	0.01781	0.01614	0.01848
011	0.01588	0.01964	0.01103	0.01986	0.01255	0.01456	0.00962	0.01960
010	0.02226	0.00233	0.01939	0.01284	0.01437	0.00253	0.01327	0.01756
001	0.01972	0.01981	0.01457	0.01947	0.00956	0.01115	0.01256	0.01600
000	0.03725	0.01884	0.01988	0.01895	0.01445	0.01534	0.01185	0.01382

Fig. 1.3. The matrix of phenomenological percents of each of the 64 triplets in the DNA-sequence of triplets in the human chromosome №1 (from [Petoukhov, 2021a,b]).

	1111	1110	1101	1100	1011	1010	1001	1000	0111	0110	0101	0100	0011	0010	0001	0000
1111	CCCC	CCCA	CCAC	CCAA	CACC	CACA	CAAC	CAAA	ACCC	ACCA	ACAC	ACAA	AACC	AACA	AAAC	AAAA
1110	CCCT	CCCG	CCAT	CCAG	CACT	CACG	CAAT	CAAG	ACCT	ACCG	ACAT	ACAG	AACT	AACG	AAAT	AAAG
1101	CCTC	CCTA	CCGC	CCGA	CATC	CATA	CAGC	CAGA	ACTC	ACTA	ACGC	ACGA	AATC	AATA	AAGC	AAGA
1100	CCTT	CCTG	CCGT	CCGG	CATT	CATG	CAGT	CAGG	ACTT	ACTG	ACGT	ACGG	AATT	AATG	AAGT	AAGG
1011	CTCC	CTCA	CTAC	CTAA	CGCC	CGCA	CGAC	CGAA	ATCC	ATCA	ATAC	ATAA	AGCC	AGCA	AGAC	AGAA
1010	CTCT	CTCG	CTAT	CTAG	CGCT	CGCG	CGAT	CGAG	ATCT	ATCG	ATAT	ATAG	AGCT	AGCG	AGAT	AGAG
1001	CTTC	CTTA	CTGC	CTGA	CGTC	CGTA	CGGC	CGGA	ATTC	ATTA	ATGC	ATGA	AGTC	AGTA	AGGC	AGGA
1000	CTTT	CTTG	CTGT	CTGG	CGTT	CGTG	CGGT	CGGG	ATTT	ATTG	ATGT	ATGG	AGTT	AGTG	AGGT	AGGG
0111	TCCC	TCCA	TCAC	TCAA	TACC	TACA	TAAC	TAAA	GCCC	GCCA	GCAC	GCAA	GACC	GACA	GAAC	GAAA
0110	TCCT	TCCG	TCAT	TCAG	TACT	TACG	TAAT	TAAG	GCCT	GCCG	GCAT	GCAG	GACT	GACG	GAAT	GAAG
0101	TCTC	TCTA	TCGC	TCGA	TATC	TATA	TAGC	TAGA	GCTC	GCTA	GCGC	GCGA	GATC	GATA	GAGC	GAGA
0100	TCTT	TCTG	TCGT	TCGG	TATT	TATG	TAGT	TAGG	GCTT	GCTG	GCGT	GCGG	GATT	GATG	GAGT	GAGG
0011	TTCC	TTCA	TTAC	TTAA	TGCC	TGCA	TGAC	TGAA	GTCC	GTCA	GTAC	GTAA	GGCC	GGCA	GGAC	GGAA
0010	TTCT	TTCG	TTAT	TTAG	TGCT	TGCG	TGAT	TGAG	GTCT	GTCC	GTAT	GTAG	GGCT	GGCG	GGAT	GGAG
0001	TTTC	TTTA	TTGC	TTGA	TGTC	TGTA	TGGC	TGGA	GTTC	GTTA	GTGC	GTGA	GGTC	GGTA	GGGC	GGGA
0000	TTTT	TTTG	TTGT	TTGG	TGTT	TGTG	TGGT	TGGG	GTTT	GTTG	GTGT	GTGG	GGTT	GGTG	GGGT	GGGG

	1111	1110	1101	1100	1011	1010	1001	1000	0111	0110	0101	0100	0011	0010	0001	0000
1111	.0033	.0055	.0042	.0044	.0040	.0056	.0032	.0070	.0030	.0042	.0040	.0053	.0032	.0059	.0055	.0149
1110	.0041	.0010	.0044	.0058	.0047	.0010	.0040	.0044	.0041	.0005	.0051	.0054	.0047	.0006	.0095	.0071
1101	.0050	.0029	.0008	.0006	.0036	.0039	.0049	.0059	.0037	.0032	.0006	.0006	.0040	.0070	.0037	.0066
1100	.0048	.0058	.0006	.0009	.0057	.0047	.0045	.0058	.0049	.0044	.0007	.0007	.0071	.0057	.0049	.0047
1011	.0052	.0057	.0027	.0038	.0010	.0006	.0003	.0006	.0033	.0045	.0032	.0063	.0042	.0049	.0039	.0078
1010	.0058	.0009	.0035	.0028	.0007	.0003	.0005	.0008	.0049	.0005	.0064	.0035	.0046	.0007	.0049	.0059
1001	.0048	.0036	.0046	.0051	.0005	.0004	.0008	.0006	.0047	.0056	.0033	.0050	.0031	.0037	.0047	.0057
1000	.0073	.0044	.0053	.0058	.0006	.0010	.0005	.0010	.0096	.0040	.0051	.0044	.0046	.0047	.0040	.0041
0111	.0046	.0049	.0042	.0051	.0024	.0045	.0028	.0078	.0030	.0041	.0029	.0038	.0023	.0037	.0029	.0073
0110	.0057	.0006	.0051	.0052	.0037	.0004	.0056	.0036	.0047	.0008	.0033	.0046	.0030	.0005	.0046	.0048
0101	.0057	.0040	.0005	.0006	.0030	.0055	.0026	.0041	.0032	.0027	.0006	.0005	.0025	.0031	.0032	.0057
0100	.0068	.0058	.0006	.0006	.0070	.0039	.0032	.0029	.0037	.0048	.0006	.0008	.0041	.0036	.0036	.0051
0011	.0051	.0063	.0034	.0063	.0041	.0049	.0031	.0061	.0023	.0031	.0017	.0035	.0031	.0042	.0023	.0052
0010	.0077	.0006	.0063	.0038	.0049	.0006	.0045	.0057	.0038	.0004	.0032	.0027	.0042	.0010	.0034	.0052
0001	.0073	.0078	.0038	.0051	.0037	.0046	.0042	.0051	.0030	.0028	.0029	.0042	.0023	.0024	.0030	.0046
0000	.0150	.0072	.0055	.0045	.0059	.0057	.0043	.0054	.0055	.0032	.0040	.0042	.0032	.0039	.0030	.0033

Fig. 1.4. The matrix of percents of each of the 256 tetraplets in the 4-text of DNA in the human chromosome №1. The upper matrix shows the distribution of 256 tetraplets in the matrix $[C, A; T, G]^{(4)}$, and the corresponding cells of the lower matrix show their phenomenological percentages (from [Petoukhov, 2021a,b]).

The regularities outlined below, illustrated on the numerical data of the single-stranded DNA sequence of the human chromosome No. 1, are also valid - according to the author's research - for a wide class of other single-stranded DNA sequences in eukaryotic and prokaryotic genomes, including the following:

- 1) all 24 human chromosomes;
- 2) all chromosomes of *Drosophila*, mouse, worm, many plants;
- 3) 19 genomes of bacteria and archaea;
- 4) many extremophiles living in extreme conditions, for example, radiation with a level 1000 times higher than fatal for humans.

The numerical data of the analysis of these DNA sequences are presented in [Petoukhov, 2020a-c, 2021a-c]).

One should remind also the origin of the symbolic $(2^n \times 2^n)$ -matrices of the n -plets alphabets in Figs. 1.1-1.4 where all rows and columns are enumerated by 2^n -bit binary numbers. These matrices are initially constructed as corresponding square tables on the bases of binary-oppositional molecular indicators in the alphabet of 4 nucleotides C, A, T, and G [Petoukhov, 2008a, 2021b; Petoukhov, He, 2010]:

- 1) Two of these molecules are purines with two rings (A and G), and the other two are pyrimidines with one ring (C and T). In terms of these oppositional indicators, **C = T = 1, A = G = 0**;
- 2) Two of these 4 nucleotides are keto molecules (T and G), and the other two - amino molecules (C and A). In terms of these oppositional indicators, **C = A = 1, T = G = 0**.

In the DNA alphabet of 4 nucleotides, each of the nucleotides C, A, T, and G is uniquely determined by its mentioned binary indicators. With this in mind, it is convenient to present sets of 4 DNA nucleotides, their 16 doublets, 64 triplets, 256 tetraplets, and so on in the form of square symbolic tables, whose columns are numbered with binary indicators "pyrimidine or purine" (**C = T = 1, A = G = 0**), and whose rows are numbered with binary indicators "amino or keto" (**C = A = 1, T = G = 0**). In such tables, all 4 nucleotides, 16 doublets, 64 triplets, 256 tetraplets of DNA automatically occupy their individual places in strict order as is shown in Figs. 1.1-1.4. These tables are not simple tables but they form a single tensor family of matrices $[C, A; T, G]^{(n)}$ where (n) refers to the tensor power. [Petoukhov, 2008; Petoukhov, He, 2010]. Below we will return to these matrices with shown binary numerations of their rows and columns many times to describe phenomenological rules of percentages of n -plets in n -texts of a genomic DNA.

2. Tensor interrelations of the percentage of oligomers in n-texts of the genomic DNA

At first glance, the sets of phenomenological percents in the different matrices in Figs. 1.1-1.4 are not numerically related to each other. In particular, one could try to use the tensor family of percentage matrices $[\%C, \%A; \%T, \%G]^{(n)} = [0.2085, 0.2910; 0.2918, 0.2087]^{(n)}$ - on the basis of the matrix of nucleotides percents from Fig. 1.1 - as a model of the interrelations between these sets in corresponding n-texts of a genomic DNA. But, as occurred, such model sets of percents of doublets, triplets, and tetraplets differ significantly from the phenomenological ones. In particular, this model $[\%C, \%A; \%T, \%G]^{(n)}$ predicts that n-plets of identical letter compositions should have identical probabilities in a corresponding genomic n-text. For example, doublets CG and GC, having the same letter composition, should have the following identical percents in the DNA of the human chromosome №1 under such model: $\%CG = \%C * \%G = 0.2085 * 0.2087 = 0.0435$, and $\%G * \%C = \%G * \%C = 0.2087 * 0.2085 = 0.0435$. But in the reality, their phenomenological percents are equal to the following values, which differ several times: $\%CG = 0.0103$, and $\%GC = 0.0440$. In addition, total sums of percentages of n-plets in each of the rows and each of the columns of a concrete model matrix $[0.2085, 0.2910; 0.2918, 0.2087]^{(n)}$ should be practically identical but matrices of real percentages have not such features at all. Briefly speaking, this model $[\%C, \%A; \%T, \%G]^{(n)}$ does not correspond to reality.

The author found another model approach on the basis of the tensor product, which discovered hidden numerical interrelations among the sets of phenomenological percents not only in the different matrices in Figs. 1.1-1.4 but also in corresponding matrices of percents of n-plets in n-texts with higher value n (in a general case, $n = 1, 2, 3, 4, 5, 6, \dots$ but not too large). Let us explain now this approach and its results.

Let us consider the vector $[C, A, G, T]$ as a sum of four sparsed vectors having 3 zero coordinates and only one non-zero coordinate (2.1):

$$[C, A, G, T] = [C, 0, 0, 0] + [0, A, 0, 0] + [0, 0, G, 0] + [0, 0, 0, T] \quad (2.1)$$

By analogy, each of the 4^n -dimensional vectors from the tensor family of vectors $[C, A, G, T]^{(n)}$ can be also represented as a sum of 4^n sparsed vectors having $4^n - 1$ zero coordinates and only one non-zero coordinate. For such representation, we will use brief denotations of the following type: $[C] = [C, 0, 0, 0]$; $[A] = [0, A, 0, 0]$; $[G] = [0, 0, G, 0]$; $[T] = [0, 0, 0, T]$; $[CC] = [CC, 0, 0, 0, 0, 0, 0, 0, 0, 0, 0, 0, 0, 0, 0, 0]$; $[AG] = [0, 0, 0, 0, 0, 0, AG, 0, 0, 0, 0, 0, 0, 0, 0, 0]$; and so on. In other words, 4 nucleotides C, A, T, G are presented by 4 vectors $[C]$, $[A]$, $[T]$, $[G]$; 16 doublets CC, CA, ... are presented by 16 vectors $[CC]$, $[CA]$, ...; 64 triplets CCC, CCA, ... are presented by 64 vectors $[CCC]$, $[CCA]$, ...; etc. Each of these sparsed vectors is conditionally termed a "maternal vector". Besides this, we also use the four-dimensional nucleotide tetra-vector $[C, A, T, G]$ whose components are symbols of 4 nucleotides. We consider the tensor products (both from right and/or from left) of each of the symbolic maternal vectors with the symbolic tetra-vector $[C, A, T, G]$ and its tensor powers $[C, A, T, G]^{(n)}$. Such tensor operations produce new symbolic oligomeric vectors of increased multi-dimensions in accordance with the properties of the tensor product (see Appendix I). Each of the produced symbolic vectors is conditionally termed a "daughter vector" regarding to the corresponding maternal vector. Components of this daughter vector are symbols of n-plets, each of which has its individual percent in a corresponding n-text of DNA.

It is striking and unexpected that, in the genomic DNA under consideration, the total sum of these individual percentages of all n-plet components of the daughter vector is equal with high accuracy to the percent of the n-plet of the maternal vector. Let us explain this by examples using the tensor products with the participation of the maternal vector $[C]$ presenting the cytosine C:

- $[C] \otimes [C, A, T, G] = [CC, CA, CT, CG]$ (it is the tensor product from right). Denote the total sum $\%CC + \%CA + \%CT + \%CG$ of percent of the 4 doublets in the produced 4-dimensional daughter vector by the symbol $\Sigma\%CN$, since all these doublets contain the nucleotide C at their first position (hereinafter, the symbol N denotes any of the nucleotides A, T, C, and G). Using values of individual percents of these 4 doublets from Fig. 1.2, one gets their total sum: $\Sigma\%CN = 0.05409 + 0.07274 + 0.07134 + 0.01031 \approx \mathbf{0.2085}$. But this value is equal to the percent $\%C = \mathbf{0.2085}$ of the nucleotide C in Fig. 1.1;
- $[C, A, T, G] \otimes [C] = [CC, AC, TC, GC]$ (it is the tensor product from left). Denote the total sum $\%CC + \%AC + \%TC + \%GC$ of percent of these new 4 doublets in the new 4-dimensional daughter vector by the symbol $\Sigma\%NC$, since all these doublets contain the nucleotide C at their second position. Using values of individual percents of these 4 doublets from Fig. 1.2, one gets their total sum: $\Sigma\%NC =$

- $0.05409+0.05033+0.06008+0.04402 \approx \mathbf{0.2085}$. This sum is again practically equal to the percent %C = $\mathbf{0.2085}$ of the nucleotide C in Fig. 1.1;
- $[C] \otimes [C, A, T, G]^{(2)} = [C] \otimes [CC, CA, CT, CG, AC, AA, AT, AG, TC, TA, TT, TG, GC, GA, GT, GG] = [CCC, CCA, CCT, CCG, CAC, CAA, CAT, CAG, CTC, CTA, CTT, CTG, CGC, CGA, CGT, CGG]$. Denote the total sum of percent of the 16 triplets in the 16-dimensional daughter vector %CCC+%CCA+%CCT+%CCG+%CAC+%CAA+%CAT+%CAG+%CTC+%CTA+%CTT+%CTG + %CGC+%CGA+%CGT+%CGG by the symbol $\Sigma\%CNN$, since all these triplets contain the nucleotide C at their first position. Using values of individual percents of these 16 triplets from Fig. 1.3, one gets their total sum: $\Sigma\%CNN = 0.01385+0.01878+0.01853+0.00291+0.01524+0.01861+0.01789+0.02104+0.01758+0.01275+0.02009+0.02088+0.00251+0.00227+0.00259+0.00291 \approx \mathbf{0.20843}$. This sum is again practically equal to the percent %C = $\mathbf{0.2085}$ of the nucleotide C in Fig. 1.1;
 - $[C, A, T, G]^{(2)} \otimes [C] = [CC, CA, CT, CG, AC, AA, AT, AG, TC, TA, TT, TG, GC, GA, GT, GG] \otimes [C] = [CCC, CAC, CTC, CGC, ACC, AAC, ATC, AGC, TCC, TAC, TTC, TGC, GCC, GAC, GTC, GGC]$. Denote the total sum %CCC+%CAC+%CTC+%CGC++%ACC+%AAC+%ATC+%AGC+%TCC+%TAC+%TTC+%TGC+%GCC+%GAC+%GTC+%GGC of percent of the 16 triplets in the new 16-dimensional daughter vector by the symbol $\Sigma\%NNC$, since all these triplets contain the nucleotide C at their third position. Using values of individual percents of these 16 triplets from Fig. 1.3, one gets their total sum: $\Sigma\%NNC = 0.01385+0.01524+0.01758+0.00251+0.01183+0.01447+0.01317+0.01441+0.01588+0.01103+0.01972+0.01457+0.01255+0.00962+0.00956+0.01256 \approx \mathbf{0.2085}$. This sum is again practically equal to the percent %C = $\mathbf{0.2085}$ of the nucleotide C in Fig. 1.1;
 - $[C, A, T, G] \otimes [C] \otimes [C, A, T, G] = [CC, AC, TC, GC] \otimes [C, A, T, G] = [CCC, CCA, CCT, CCG, ACC, ACA, ACT, ACG, TCC, TCA, TCT, TCG, GCC, GCA, GCT, GCG]$. Denote the total sum %CCC+%CCA+%CCT+%CCG+%ACC+%ACA+%ACT+%ACG+%TCC+%TCA+%TCT+%TCG+ %GCC+%GCA+%GCT+%GCG of percent of these 16 triplets in the new 16-dimensional daughter vector by the symbol $\Sigma\%NCN$ since all these triplets contain the nucleotide C at their second position. Using values of individual percents of the 16 triplets from Fig. 1.3, one gets their total sum: $\Sigma\%NCN = 0.01385+0.01878+0.01853+0.00291+0.01183+0.01977+0.01622+0.00254+0.01588+0.01964+0.0222+0.00233+0.01255+0.01456+0.01437+0.00253 = \mathbf{0.2085}$. This sum is again practically equal to the percent %C $\approx \mathbf{0.2085}$ of the nucleotide C in Fig. 1.1;
 - $[C] \otimes [C, A, T, G]^{(3)} = [CCC, CCA, CCT, CCG, CAC, CAA, CAT, CAG, CTC, CTA, CTT, CTG, CGC, CGA, CGT, CGG] \otimes [C, A, T, G] = [CCCC, CCCA, CCCT, CCCG, CCAC, CCAA, CCAT, CCAG, CCTC, CCTA, CCTT, CCTG, CCGC, CCGA, CCGT, CCGG, CACC, CACA, CACT, CACG, CAAC, CAAA, CAAT, CAAG, CATC, CATA, CATT, CATG, CAGC, CAGA, CAGT, CAGG, CTCC, CTCA, CTCT, CTCG, CTAC, CTAA, CTAT, CTAG, CTTC, CTTA, CTTT, CTTG, CTGC, CTGA, CTGT, CTGG, CGCC, CGCA, CGCT, CGCG, CGAC, CGAA, CGAT, CGAG, CGTC, CGTA, CGTT, CGTG, CGGC, CGGA, CGGT, CGGG]$. Denote the total sum of percent of these 64 tetraplets in the 64-dimensional daughter vector by the symbol $\Sigma\%CNNN$ since all these tetraplets contain the nucleotide C at their first position. Using values of individual percents of the 64 tetraplets from Fig. 1.4, one can calculate their total sum: $\Sigma\%CNNN \approx \mathbf{0.2085}$. This sum is again practically equal to the percent %C = $\mathbf{0.2085}$ of the nucleotide C in Fig. 1.1;
 - $[C, A, T, G] \otimes [C] \otimes [C, A, T, G]^{(2)} = [C, A, T, G] \otimes [CCC, CCA, CCT, CCG, CAC, CAA, CAT, CAG, CTC, CTA, CTT, CTG, CGC, CGA, CGT, CGG] = [CCCC, CCCA, CCCT, CCCG, CCAC, CCAA, CCAT, CCAG, CCTC, CCTA, CCTT, CCTG, CCGC, CCGA, CCGT, CCGG, ACCC, ACCA, ACCT, ACCG, ACAC, ACAA, ACAT, ACAG, ACTC, ACTA, ACTT, ACTG, ACGC, ACGA, ACGT, ACGG, TCCC, TCCA, TCCT, TCCG, TCAC, TCAA, TCAT, TCAG, TCTC, TCTA, TCTT, TCTG, TCGC, TCGA, TCGT, TCGG, GCCC, GCCA, GCCT, GCCG, GCAC, GCAA, GCAT, GCAG, GCTC, GCTA, GCTT, GCTG, GCGC, GCGA, GCGT, GCGG]$. Denote the total sum of percent of these 64 tetraplets in the 64-dimensional daughter vector by the symbol $\Sigma\%NCNN$ since all these tetraplets contain the nucleotide C at their second position. Using values of individual percents of the 64 tetraplets from Fig. 1.4, one can calculate their total sum: $\Sigma\%NCNN \approx \mathbf{0.2085}$. This sum is again practically equal to the percent %C = $\mathbf{0.2085}$ of the nucleotide C in Fig. 1.1;
 - $[C, A, T, G]^{(2)} \otimes [C] \otimes [C, A, T, G] = [CCC, CAC, CTC, CGC, ACC, AAC, ATC, AGC, TCC, TAC, TTC, TGC, GCC, GAC, GTC, GGC] \otimes [C, A, T, G] = [CCCC, CCCA, CCCT, CCCG, CACC, CACA, CACT, CACG, CTCC, CTCA, CTCT, CTCG, CGCC, CGCA, CGCT, CGCG, ACCC, ACCA, ACCT,$

ACCG, AACC, AACA, AACT, AACG, ATCC, ATCA, ATCT, ATCG, AGCC, AGCA, AGCT, AGCG, TCCC, TCCA, TCCT, TCCG, TACC, TACA, TACT, TACG, TTCC, TTCA, TTCT, TTCG, TGCC, TGCA, TGCT, TGCG, GCCC, GCCA, GCCT, GCCG, GACC, GACA, GACT, GACG, GTCC, GTCA, GTCT, GTCG, GGCC, GGCA, GGCT, GGCG]. Denote the total sum of percent of these 64 tetraplets in the 64-dimensional daughter vector by the symbol $\Sigma\%NNCN$ since all these tetraplets contain the nucleotide C at their third position. Using values of individual percents of the 64 tetraplets from Fig. 1.4, one can calculate their total sum: $\Sigma\%NNCN \approx 0.2085$. This sum is again practically equal to the percent $\%C = 0.2085$ of the nucleotide C in Fig. 1.1;

- $[C, A, T, G]^{(3)} \otimes [C] = [CCCC, CCAC, CCTC, CCGC, CACC, CAAC, CATC, CAGC, CTCC, CTAC, CTTC, CTGC, CGCC, CGAC, CGTC, CGGC, ACCC, ACAC, ACTC, ACGC, AACC, AAAC, AATC, AAGC, ATCC, ATAC, ATTC, ATGC, AGCC, AGAC, AGTC, AGGC, TCCC, TCAC, TCTC, TCGC, TACC, TAAC, TATC, TAGC, TTCC, TTAC, TTTC, TTGC, TGCC, TGAC, TGTC, TGGC, GCCC, GCAC, GCTC, GCGC, GACC, GAAC, GATC, GAGC, GTCC, GTAC, GTTC, GTGC, GGCC, GGAC, GGTC, GGGC]$. Denote the total sum of percent of these 64 tetraplets in the 64-dimensional daughter vector by the symbol $\Sigma\%NNNC$ since all these tetraplets contain the nucleotide C at their fourth position. Using values of individual percents of the 64 tetraplets from Fig. 1.4, one can calculate their total sum: $\Sigma\%NNNC \approx 0.2085$. This sum is again practically equal to the percent $\%C = 0.2085$ of the nucleotide C in Fig. 1.1.
- etc.

Similar numeric equalities hold for genomic DNA in cases of the maternal vectors of nucleotides [A], [T], and [G] under their tensor product (both from the right and from the left) with the tetra-vector of nucleotides [C, A, T, G]: the total sum of individual percentages of all n-plets components of the daughter vector is equal with high accuracy to the percent of the nucleotide in the maternal vector. By analogy, in these cases we have the following tensor products:

- In the case of the maternal vector [A]: $[A] \otimes [C, A, T, G], [C, A, T, G] \otimes [A], [A] \otimes [C, A, T, G]^{(2)}, [C, A, T, G]^{(2)} \otimes [A], [C, A, T, G] \otimes [A] \otimes [C, A, T, G], [A] \otimes [C, A, T, G]^{(3)}, [C, A, T, G] \otimes [A] \otimes [C, A, T, G]^{(2)}, [C, A, T, G]^{(2)} \otimes [A] \otimes [C, A, T, G], [C, A, T, G]^{(3)} \otimes [A]$. These tensor products lead to corresponding total sums of percent of components of daughter vectors: $\Sigma\%AN, \Sigma\%NA, \Sigma\%ANN, \Sigma\%NNA, \Sigma\%NAN, \Sigma\%ANNN, \Sigma\%NANN, \Sigma\%NNAN, \Sigma\%NNNA$. Each of these sums is practically equal to the percent of the nucleotide A: $\%A = 0.2910$ (from Fig. 1.1);
- In the case of the maternal vector [T]: $[T] \otimes [C, A, T, G], [C, A, T, G] \otimes [T], [T] \otimes [C, A, T, G]^{(2)}, [C, A, T, G]^{(2)} \otimes [T], [C, A, T, G] \otimes [T] \otimes [C, A, T, G], [T] \otimes [C, A, T, G]^{(3)}, [C, A, T, G] \otimes [T] \otimes [C, A, T, G]^{(2)}, [C, A, T, G]^{(2)} \otimes [T] \otimes [C, A, T, G], [C, A, T, G]^{(3)} \otimes [T]$. These tensor products lead to corresponding total sums of percent of components of daughter vectors: $\Sigma\%TN, \Sigma\%NT, \Sigma\%TNN, \Sigma\%NNT, \Sigma\%NTN, \Sigma\%TNNN, \Sigma\%NTNN, \Sigma\%NNTN, \Sigma\%NNNT$. Each of these sums is practically equal to the percent of the nucleotide T: $\%T = 0.2918$ (from Fig. 1.1);
- In the case of the maternal vector [G]: $[G] \otimes [C, A, T, G], [C, A, T, G] \otimes [G], [G] \otimes [C, A, T, G]^{(2)}, [C, A, T, G]^{(2)} \otimes [G], [C, A, T, G] \otimes [G] \otimes [C, A, T, G], [G] \otimes [C, A, T, G]^{(3)}, [C, A, T, G] \otimes [G] \otimes [C, A, T, G]^{(2)}, [C, A, T, G]^{(2)} \otimes [G] \otimes [C, A, T, G], [C, A, T, G]^{(3)} \otimes [G]$. These tensor products lead to corresponding total sums of percent of components of daughter vectors: $\Sigma\%GN, \Sigma\%NG, \Sigma\%GNN, \Sigma\%NNG, \Sigma\%NGN, \Sigma\%GNNN, \Sigma\%NGNN, \Sigma\%NNGN, \Sigma\%NNNG$. Each of these sums is practically equal to the percent of the nucleotide G: $\%G = 0.2087$ (from Fig. 1.1).

A summary table of these amounts and equalities is shown in Fig. 2.1.

$\%C \approx 0.2085$	$\%G \approx 0.2087$	$\%A \approx 0.2910$	$\%T \approx 0.2918$
$\Sigma\%CN \approx 0.2085$	$\Sigma\%GN \approx 0.2088$	$\Sigma\%AN \approx 0.2910$	$\Sigma\%TN \approx 0.2917$
$\Sigma\%NC \approx 0.2085$	$\Sigma\%NG \approx 0.2087$	$\Sigma\%NA \approx 0.2910$	$\Sigma\%NT \approx 0.2918$

$\Sigma\%CNN \approx 0.2084$	$\Sigma\%GNN \approx 0.2088$	$\Sigma\%ANN \approx 0.2910$	$\Sigma\%TNN \approx 0.2917$
$\Sigma\%NCN \approx 0.2085$	$\Sigma\%NGN \approx 0.2088$	$\Sigma\%NAN \approx 0.2910$	$\Sigma\%NTN \approx 0.2917$
$\Sigma\%NNC \approx 0.2085$	$\Sigma\%NNG \approx 0.2087$	$\Sigma\%NNA \approx 0.2910$	$\Sigma\%NNT \approx 0.2918$
$\Sigma\%CNNN \approx 0.2085$	$\Sigma\%GNNN \approx 0.2088$	$\Sigma\%ANNN \approx 0.2910$	$\Sigma\%TNNN \approx 0.2917$
$\Sigma\%NCNN \approx 0.2085$	$\Sigma\%NGNN \approx 0.2087$	$\Sigma\%NANN \approx 0.2910$	$\Sigma\%NTNN \approx 0.2918$
$\Sigma\%NNCN \approx 0.2085$	$\Sigma\%NNGN \approx 0.2088$	$\Sigma\%NNAN \approx 0.2910$	$\Sigma\%NNTN \approx 0.2918$
$\Sigma\%NNNC \approx 0.2085$	$\Sigma\%NNNG \approx 0.2087$	$\Sigma\%NNNA \approx 0.2910$	$\Sigma\%NNNT \approx 0.2918$
♠	♣	♥	♦

Fig. 2.1. The four columns show corresponding tetra-groupings of percentages of nucleotides C, G, A, T jointly with the sums Σ of percent of n -plets, having these nucleotides at certain positions, for the case of n -texts of the DNA of the human chromosome №1 (from [Petoukhov, 2021a,b]). The symbol N denotes any of the nucleotides. Four playing card symbols are used for denotations of n -plets in these four columns.

Fig. 2.1 shows tetra-groupings of the sums of genomic percentages of n -plets in n -texts of the considered DNA. Taking into account the belonging of each n -plet to one of the 4 columns, that is, to one of the C-, G-, A-, and T-groupings, we introduce the following symbolic notation for each of the n -plets:

- n -plets of the first column (C-column) are denoted by the symbol ♠;
- n -plets of the second column (G-column) are denoted by the symbol ♣;
- n -plets of the third column (A-column) are denoted by the symbol ♥;
- n -plets of the fourth column (T-column) are denoted by the symbol ♦.

This denotation by four playing card symbols will be useful below in the section about Rademacher functions, which are closely connected with the theory of probabilities.

Above we described genomic stochastic rules in the cases of maternal vectors [C], [A], [T], and [G] on the basis of 4 nucleotides. But similar genomic stochastic rules exist in cases of maternal vectors on the basis of all 16 doublets ([CC], [CA], ...), and on the basis of all 64 triplets ([CCC], [CCA], ...), and so on regarding results of their tensor product (both from the right and from the left) with the tetra-vector [C, A, T, G]. Let us initially demonstrate this for a case of the maternal vector [CC] in the human chromosome №1:

- $[CC] \otimes [C, A, T, G] = [CCC, CCA, CCT, CCG]$. Denote the total sum $\%CCC + \%CCA + \%CCT + \%CCG$ of percent of the 4 triplets in the produced 4-dimensional daughter vector by the symbol $\Sigma\%CCN$ since all these triplets contain the doublet CC at their first positions. Using values of individual percents of these 4 triplets from Fig. 1.3, one gets their total sum: $\Sigma\%CCN = 0.01385 + 0.01878 + 0.01853 + 0.00291 \approx 0.05407$. This sum is practically equal to the percent $\%CC = 0.05409$ of the doublet CC in Fig. 1.2;
- $[C, A, T, G] \otimes [CC] = [CCC, ACC, TCC, GCC]$. Denote the total sum $\%CCC + \%ACC + \%TCC + \%GCC$ of percent of the 4 triplets in the produced 4-dimensional daughter vector by the symbol $\Sigma\%NCC$ since all these triplets contain the doublet CC at their end positions. Using values of individual percents of these 4 triplets from Fig. 1.3, one gets their total sum: $\Sigma\%NCC = 0.01385 + 0.01183 + 0.01588 + 0.01255 \approx 0.05411$. This sum is practically equal again to the percent $\%CC = 0.05409$ of the doublet CC in Fig. 1.2;
- $[CC] \otimes [C, A, T, G]^{(2)} = [CCCC, CCCA, CCCT, CCCG, CCAC, CCAA, CCAT, CCAG, CCTC, CCTA, CCTT, CCTG, CCGC, CCGA, CCGT, CCGG]$. Denote the total sum of percent of these 16 tetraplets in the produced 16-dimensional daughter vector by the symbol $\Sigma\%CCNN$ since all these tetraplets contain the doublet CC at their first positions. Using values of individual percents of these 16 tetraplets from Fig. 1.4, one can calculate their total sum: $\Sigma\%CCNN \approx 0.0033 + 0.0055 + 0.0041 + 0.0010 + 0.0042 + 0.0044 + 0.0044 + 0.0058 + 0.0050 + 0.0029 + 0.0048 + 0.0058 + 0.0008 + 0.0006 + 0.0006 + 0.0009 \approx 0.0541$. This sum is practically equal again to the percent $\%CC = 0.05409$ of the doublet CC in Fig. 1.2;
- $[C, A, T, G] \otimes [CC] \otimes [C, A, T, G] = [CCCC, CCCA, CCCT, CCCG, ACCC, ACCA, ACCT, ACCG, TCCC, TCCA, TCCT, TCCG, GCCC, GCCA, GCCT, GCCG]$. Denote the total sum of percent of these 16 tetraplets in the produced 16-dimensional daughter vector by the symbol $\Sigma\%NCCN$ since all these tetraplets contain the doublet CC at their middle positions. Using values of individual percents of these

16 tetraplets from Fig. 1.4, one can calculate their total sum: $\Sigma \%NCCN \approx 0.0033+0.0055+0.0041+0.0010+0.0030+0.0042+0.0041+0.0005+0.0046+0.0049+0.0057+0.0006+0.0030+0.0041+0.0047+0.0008 \approx \mathbf{0.0541}$. This sum is practically equal to the percent $\%CC = \mathbf{0.05409}$ of the doublet CC in Fig. 1.2;

- $[C, A, T, G]^{(2)} \otimes [CC] = [CCCC, CACC, CTCC, CGCC, ACCC, AACC, ATCC, AGCC, TCCC, TACC, TTCC, TGCC, GCCC, GACC, GTCC, GGCC]$. Denote the total sum of percent of these 16 tetraplets in the produced 16-dimensional daughter vector by the symbol $\Sigma\%NNCC$ since all these tetraplets contain the doublet CC at their end positions. Using values of individual percents of these 16 tetraplets from Fig. 1.4, one can calculate their total sum: $\Sigma \%NNCC \approx 0.0033+0.0040+0.0052+0.0010+0.0030+0.0032+0.0033+0.0042+0.0046+0.0024+0.0051+0.0041+0.0030+0.0023+0.0023+0.0031 \approx \mathbf{0.0541}$. This sum is practically equal to the percent $\%CC = \mathbf{0.05409}$ of the doublet CC in Fig. 1.2.

Similar numeric equalities hold for genomic DNA in cases of the maternal vectors of other 15 doublets [CA], [CT], [CG], [AC], [AA], [AT], [AG], [TC], [TA], [TT], [TG], [GC], [GA], [GT], [GG] under their tensor product (both from the right and from the left) with the tetra-vector of nucleotides [C, A, T, G]: in each of these cases, the total sum of individual percentages of all oligomeric components of the daughter vector is equal with high accuracy to the percent of the doublet in the maternal vector.

A summary table of corresponding amounts and equalities is shown in Fig. 2.2.

$\%AA \approx \Sigma\%AAN \approx \Sigma\%NAA \approx \Sigma\%AANN \approx \Sigma\%NAAN \approx \Sigma\%NNA A \approx 0.095$
$\%AT \approx \Sigma\%ATN \approx \Sigma\%NAT \approx \Sigma\%ATNN \approx \Sigma\%NATN \approx \Sigma\%NNAT \approx 0.074$
$\%AC \approx \Sigma\%ACN \approx \Sigma\%NAC \approx \Sigma\%ACNN \approx \Sigma\%NACN \approx \Sigma\%NNAC \approx 0.050$
$\%AG \approx \Sigma\%AGN \approx \Sigma\%NAG \approx \Sigma\%AGNN \approx \Sigma\%NAGN \approx \Sigma\%NNAG \approx 0.071$
$\%TA \approx \Sigma\%TAN \approx \Sigma\%NTA \approx \Sigma\%TANN \approx \Sigma\%NTAN \approx \Sigma\%NNTA \approx 0.063$
$\%TT \approx \Sigma\%TTN \approx \Sigma\%NTT \approx \Sigma\%TTNN \approx \Sigma\%NTTN \approx \Sigma\%NNTT \approx 0.096$
$\%TC \approx \Sigma\%TCN \approx \Sigma\%NTC \approx \Sigma\%TCNN \approx \Sigma\%NTCN \approx \Sigma\%NNTC \approx 0.060$
$\%TG \approx \Sigma\%TGN \approx \Sigma\%NTG \approx \Sigma\%TGNN \approx \Sigma\%NTGN \approx \Sigma\%NNTG \approx 0.073$
$\%CA \approx \Sigma\%CAN \approx \Sigma\%NCA \approx \Sigma\%CANN \approx \Sigma\%NCAN \approx \Sigma\%NNCA \approx 0.073$
$\%CT \approx \Sigma\%CTN \approx \Sigma\%NCT \approx \Sigma\%CTNN \approx \Sigma\%NCTN \approx \Sigma\%NNCT \approx 0.071$
$\%CC \approx \Sigma\%CCN \approx \Sigma\%NCC \approx \Sigma\%CCNN \approx \Sigma\%NCCN \approx \Sigma\%NNCC \approx 0.054$
$\%CG \approx \Sigma\%CGN \approx \Sigma\%NCG \approx \Sigma\%CGNN \approx \Sigma\%NCGN \approx \Sigma\%NNCG \approx 0.010$
$\%GA \approx \Sigma\%GAN \approx \Sigma\%NGA \approx \Sigma\%GANN \approx \Sigma\%NGAN \approx \Sigma\%NNGA \approx 0.060$
$\%GT \approx \Sigma\%GTN \approx \Sigma\%NGT \approx \Sigma\%GTNN \approx \Sigma\%NGTN \approx \Sigma\%NNGT \approx 0.050$
$\%GC \approx \Sigma\%GCN \approx \Sigma\%NGC \approx \Sigma\%GCNN \approx \Sigma\%NGCN \approx \Sigma\%NNGC \approx 0.044$
$\%GG \approx \Sigma\%GGN \approx \Sigma\%NGG \approx \Sigma\%GGNN \approx \Sigma\%NGGN \approx \Sigma\%NNGG \approx 0.054$

Fig. 2.2. Percentage sums are presented for *mm*-positional tetra-groupings related to 64 triplets and 256 tetraplets in the appropriate 3-text and 4-text of the DNA of the human chromosome №1 (from [Petoukhov, 2021a,b]). Each of these tetra-groupings is defined by one of 16 doublets as its attributive positional element disposed of in the beginning, or in the middle, or at the end of the *n*-plets. Numerical values of percentage sums are calculated based on data about the percents of separate *n*-plets in 2-, 3-, and 4-texts of this DNA in Figs. 1.2-1.4.

Similar numeric equalities hold for genomic DNA in cases of the maternal vectors of 64 triplets [CCC], [CCA], ..., [GGG] under their tensor product (both from the right and from the left) with the tetra-vector of nucleotides [C, A, T, G]: in each of these cases, the total sum of individual percentages of all oligomeric components of the daughter vector is equal with high accuracy to the percent of the triplet in the maternal vector. For example, in the case of the maternal vector [CCC] we have the following:

- $[CCC] \otimes [C, A, T, G] = [CCCC, CCCA, CCCT, CCCG]$ (it is the tensor product from right). Using values of individual percents of these 4 tetraplets from Fig. 1.4, one gets their total sum $\%CCCC+\%CCCA+\%CCCT+\%CCCG = 0.0033+0.0055+0.0041+0.0010 = \mathbf{0.0139}$. But this sum is practically equal to the percent of the maternal triplet CCC: $\%CCC = \mathbf{0.01385}$ (from Fig. 1.3);

- $[C, A, T, G] \otimes [CCC] = [CCCC, ACCC, TCCC, GCCC]$ (it is the tensor product from left). Using values of individual percents of these 4 tetraplets from Fig. 1.4, one gets their total sum $\%CCCC + \%ACCC + \%TCCC + \%GCCC = 0.0033 + 0.0030 + 0.0046 + 0.0030 = 0.0139$. But this sum is again practically equal to the percent of the maternal triplet CCC: $\%CCC = 0.01385$ (from Fig. 1.3);

The described genomic phenomena and rules of the relative independence of the sums of the percentages of n -plets (in the indicated tetra-groupings of n -plets in genomic n -texts) from the values of individual percentages of summands in these sums are termed genetical Gestalt phenomena and rules. They are used by the author for developing Gestalt genetics in close analogy with Gestalt psychology and its genetically inherited phenomena [Petoukhov, 2021a,b].

3. Regarding the connection of the stochastic phenomenon of tetra-colonies of n -plets in genomic n -texts with quantum formalisms of vectors of probability amplitudes.

In quantum mechanics and quantum informatics, when analyzing the probabilities of events, the amplitudes of these probabilities, equal to the square root of their values, are traditionally considered. The genomic Gestalt phenomena for percentages of n -plets (in C-, G-, A-, and T-groupings) were above described under analyzing the sums of the probabilities of n -plets from certain groupings, for example, all doublets starting with the letter C ($\%CC + \%CA + \%CT + \%CG = \%C$) and all doublets ending with the letter C ($\%CC + \%AC + \%TC + \%GC = \%C$). Each of these probabilities $\%CC$, $\%CA$, $\%CT$, $\%CG$, $\%AC$, $\%TC$, and $\%GC$ has its own "amplitude" in the form of its square root.

It can be noted that the sum of the percentages (that is, the probabilities) of n -plets in each of these four groupings can be interpreted as the square of the length of a vector whose components are equal to the square roots of the probabilities of the corresponding n -plets. For example, the sum $\%CC + \%CG + \%CA + \%CT$ is the square of the length of the 4-dimensional vector $V_{CN} = [\sqrt{\%CC}, \sqrt{\%CG}, \sqrt{\%CA}, \sqrt{\%CT}]$ and the sum $\%CC + \%AC + \%TC + \%GC$ is the square of the length of another 4-dimensional vector $V_{NC} = [\sqrt{\%CC}, \sqrt{\%AC}, \sqrt{\%TC}, \sqrt{\%GC}]$. From this point of view, the phenomenological equality of the sums of percent $\%CC + \%CG + \%CA + \%CT$ and $\%CC + \%AC + \%TC + \%GC$ means the equality of the lengths of these vectors $V_{CN} = V_{NC}$, whose coordinates are the amplitudes of the probabilities of the corresponding n -plets. Such vectors of equal length can be transformed into each other by unitary transformations that do not change the length of the vectors and are either rotations or mirror reflections. A similar situation holds for the equality of the above-described sums $\Sigma\%CNN = \Sigma\%NCN = \Sigma\%NNC$, etc., which correspond to appropriate vectors of probability amplitudes having an equal length and a possibility to transform into each other by unitary transformations.

Thus, the described tensor-related phenomena of algebraic Gestalt genetics turns out to be connected with unitary operators, which are key for quantum informatics: all calculations in quantum computers and quantum search algorithms are based on unitary operators as quantum gates. Moreover, any unitary matrix can serve as a quantum gate. In quantum mechanics, the evolution of a closed quantum system is described by unitary transformations. Since this article deals with many n -texts of genomic DNA, it can be assumed that, in particular, a whole set of quantum search algorithms work in sets of such n -texts, each of which is individually oriented to a particular n -text. The articles [Patel, 2001a-c] suppose that the genetic code is related to the quantum Grover's algorithm.

Along the way, one can note that the entire genetically inherited kinematic scheme of movements of our body with its parts is built on rotations in the joints and mirror reflections, that is, on unitary transformations that have physiological significance. Turtles and crocodiles, when hatched from an egg, immediately crawl to the water with coordinated movements using innate algorithms with the same unitary transformations of rotations and mirror reflections.

The materials of this article supplement the author's previously published works on the topic of quantum biology and formalisms of quantum informatics in biology [Petoukhov, 2008, 2016, 2018, 2020a,c, 2021a-c; Petoukhov, He, 2010; Petoukhov, Petukhova, Svirin, 2019; Fimmel, Petoukhov, 2020]. The revealed connection of genetics with quantum informatics opens up the possibility of introducing rich formalisms of quantum mechanics and quantum informatics into algebraic biology for the mutual enrichment of these sciences and the inclusion of biology in the field of developed mathematical natural

science. There are about 100 trillion cells in the human body, forming a single system. The formalisms of quantum informatics and Gestalt genetics can help in understanding such coherence phenomena.

One should mention suppositions of many authors that formalisms of quantum informatics can be effectively used for deep understanding and modeling biological bodies (see, for example: [Igamberdiev, 1993; Matsuno, 1999; Matsuno, Paton, 2000; Abbott, Davies, Pati, 2008]).

4. Equality of the sums of probabilities of n-plets in binary-inversinable pairs of rows and columns of genomic probability matrices.

Above we described some hidden universal equalities of percentage sums in the matrices of the probability of n-plets in n-texts of genomic DNA. But in addition to these equalities in the stochastic n-textual organization of genomic DNA, there are also other universal phenomena of symmetry. We will describe them below using the same matrices of genomic probabilities of members of n-plets alphabets (Figs. 1.1-1.4). The whole set of revealed symmetry relations between the groupings of percentages of n-plets in genomic n-texts indicates that the stochastic n-textual organization of genomic DNA is highly limited stochastics with many internal numeric interrelations among summary percentages of separate groupings. This limited stochastic organization of genomic DNA is closely related to binary-oppositional (or Yin-Yang) principles, which is additionally illustrated in this section. Firstly, in each of the probability matrices in Figs. 1.1-1.4, let us compare percentage sums of n-plets in pairs of those columns, which are binarily enumerated by binary-inversinable numbers. We term a pair of binary-inversinable numbers those two binary numbers, which are transformed into each other by the simultaneous inversion $0 \rightarrow 1$ and $1 \rightarrow 0$ for all their binary symbols. For example, two binary numbers 1011 and 0100 are binary-inversinable.

The author draws attention to an amazing phenomenological rule in the stochastic organization of genomes: any two columns of matrices (Figs. 1.1-1.4), which are binarily enumerated with binary-inversinable numbers, have practically the same percentage sums (although the individual percentages in each of the columns are very different). Figs. 4.1-4.3 show examples of performance of this rule for percent sets in cases of 16 doublets, 64 triplets, and 256 tetraplets in n-texts of DNA of the human chromosome №1.

Columns	Percentage sums in columns
11	0.05409+0.07134+0.06008+0.09568 = 0.28119
00	0.09504+0.07137+0.06008+0.05419 = 0.28068
10	0.07274+0.01031+0.06312+0.07286 = 0.21903
01	0.05033+0.07429+0.04402+0.05046 = 0.21910

Fig. 4.1. Percentage sums in columns of the probability matrix of 16 doublets from Fig. 1.2.

Bold boxes mark pairs of columns numerated with binary-inversinable numbers shown at the left. In each of the boxes, percentage sums in both columns are practically the same.

Columns	Percentage sums in columns
111	0.01385+0.01853+0.01758+0.02009+0.01588+0.02226+0.01972+0.03725 = 0.16516
000	0.03693+0.01988+0.02237+0.01848+0.01960+0.01756+0.01600+0.01382 = 0.16464
110	0.01878+0.00291+0.01275+0.02088+0.01964+0.00233+0.01981+0.01884 = 0.11594
001	0.01447+0.02375+0.01441+0.01614+0.00962+0.01327+0.01256+0.01185 = 0.11607
101	0.01524+0.01789+0.00251+0.00259+0.01103+0.01939+0.01457+0.01988 = 0.10310
010	0.01977+0.00254+0.01942+0.01781+0.01456+0.00253+0.01115+ 0.01534 = 0.10312
100	0.01861+0.02104+0.00227+0.00291+0.01986+0.01284+0.01947+0.01895 = 0.11595
011	0.01183+0.01622+0.01317+0.02388+0.01255+0.01437+0.00956+0.01445 = 0.11603

Fig. 4.2. Percentage sums in columns of the probability matrix of 64 triplets from Fig. 1.3.

Bold boxes mark pairs of columns numerated with binary-inversinable numbers shown at the left. In each of the boxes, percentage sums in both columns are practically the same.

Columns	Percentage sums in columns
1111	0.0033+0.0041+0.0050+0.0048+0.0052+0.0058+0.0048+0.0073+0.0046+0.0057+0.0057+0.0068+0.0051+0.0077+0.0073+0.0150 = 0.0982
0000	0.0149+0.0071+0.0066+0.0047+0.0078+0.0059+0.0057+0.0041+0.0073+0.0048+0.0057+0.0051+0.0052+0.0052+0.0046+0.0033 = 0.0980
1110	0.0055+0.0010+0.0029+0.0058+0.0057+0.0009+0.0036+0.0044+0.0049+0.0006+0.0040+0.0058+0.0063+0.0006+0.0078+0.0072 = 0.0670
0001	0.0055+0.0095+0.0037+0.0049+0.0039+0.0049+0.0047+0.0040+0.0029+0.0046+0.0032+0.0036+0.0023+0.0034+0.0030+0.0030 = 0.0671
1101	0.0042+0.0044+0.0008+0.0006+0.0027+0.0035+0.0046+0.0053+0.0042+0.0051+0.0005+0.0006+0.0034+0.0063+0.0038+0.0055 = 0.0555
0010	0.0059+0.0006+0.0070+0.0057+0.0049+0.0007+0.0037+0.0047+0.0037+0.0005+0.0031+0.0036+0.0042+0.0010+0.0024+0.0039 = 0.0556
1100	0.0044+0.0058+0.0006+0.0009+0.0038+0.0028+0.0051+0.0058+0.0051+0.0052+0.0006+0.0006+0.0063+0.0038+0.0051+0.0045 = 0.0604
0011	0.0032+0.0047+0.0040+0.0071+0.0042+0.0046+0.0031+0.0046+0.0023+0.0030+0.0025+0.0041+0.0031+0.0042+0.0023+0.0032 = 0.0602
1011	0.0040+0.0047+0.0036+0.0057+0.0010+0.0007+0.0005+0.0006+0.0024+0.0037+0.0030+0.0070+0.0041+0.0049+0.0037+0.0059 = 0.0555
0100	0.0053+0.0054+0.0006+0.0007+0.0063+0.0035+0.0050+0.0044+0.0038+0.0046+0.0005+0.0008+0.0035+0.0027+0.0042+0.0042 = 0.0555
1010	0.0056+0.0010+0.0039+0.0047+0.0006+0.0003+0.0004+0.0010+0.0045+0.0004+0.0055+0.0039+0.0049+0.0006+0.0046+0.0057 = 0.0476
0101	0.0040+0.0051+0.0006+0.0007+0.0032+0.0064+0.0033+0.0051+0.0029+0.0033+0.0006+0.0006+0.0017+0.0032+0.0029+0.0040 = 0.0476
1001	0.0032+0.0040+0.0049+0.0045+0.0003+0.0005+0.0008+0.0005+0.0028+0.0056+0.0026+0.0032+0.0031+0.0045+0.0042+0.0043 = 0.0490
0110	0.0042+0.0005+0.0032+0.0044+0.0045+0.0005+0.0056+0.0040+0.0041+0.0008+0.0027+0.0048+0.0031+0.0004+0.0028+0.0032 = 0.0488
1000	0.0070+0.0044+0.0059+0.0058+0.0006+0.0008+0.0006+0.0010+0.0078+0.0036+0.0041+0.0029+0.0061+0.0057+0.0051+0.0054 = 0.0668
0111	0.0030+0.0041+0.0037+0.0049+0.0033+0.0049+0.0047+0.0096+0.0030+0.0047+0.0032+0.0037+0.0023+0.0038+0.0030+0.0055 = 0.0674

Fig. 4.3. Percentage sums in columns of the probability matrix of 256 tetraplets from Fig. 1.4.

Bold boxes mark pairs of columns enumerated with binary-inversible numbers shown at the left. In each of the boxes, percentage sums in both columns are practically the same.

One should remind that binary numeration of columns uses the following denotations as it was above-explained in the Introduction: the binary symbol **1** denotes pyrimidines (C or T) and the binary symbol **0** denotes purines (A or G). Correspondingly, each of the columns of any such matrices (like in Figs. 1.1-1.4) contains all n-plets having an identical sequence of pyrimidines and purines. For example, in the matrix of 64 triplets in Fig. 1.3, the column with its binary numeration **011** contains all 8 triplets with the identical sequence “**purine-pyrimidine-pyrimidine**”: ACC, ACT, ATC, ATT, GCC, GCT, GTC, and GTT. The column having the binary-inverse numeration **100** contains all 8 triplets with the sequence of the opposite type “**pyrimidine-purine-purine**”: CAA, CAG, CGA, CGG, TAA, TAG, TGA, and TGG. Each of the triplets of the first sequence is complementary with one of the triplets of the second sequence: ACC is complementary with TGG; ACT – with TGA; ATC – with TAG; ATT – with TAA; GCC – with CGG; GCT – with CGA; GTC – with CAG; GTT – with CAA (here the complementary is understood in the sense of the complementary of oligomers in the DNA double helix). We term such pairs of sequences as “complementary sequences” relative to indicators “purine-or-pyrimidine”. In the considered matrix of 64 triplets (Fig. 1.3), these complementary

triplets are located inversion-symmetrical relative to the center of the matrix. Similar is true for locations of complementary n-plets in columns having the binary-inversible numerations in other considered matrices (Figs. 1.1, 1.2, 1.4).

The described phenomenological facts, whose separate examples are represented in Figs. 4.1-4.3, about the equalities of total percentage sums of all n-plets in the noted subsets on the bases of the binary indicators “purine-or-pyrimidine” can be expressed by the following rule, which is a candidacy for a role of the universal genetic rule:

- In any n-text of DNA of eukaryotic and prokaryotic genomes, a total percentage sum of all those n-plets, whose molecular contents are identical to each other relative to some sequence of purines and pyrimidines, is approximately equal to a total percentage sum of all those n-plets, whose molecular contents are identical relative to the complementary sequence of pyrimidines and purines (although the individual percentages of the corresponding n-plets in the considered complementary sequences can differ significantly from each other, as can be seen from Figs. 4.1-4.3).

For this rule, as usual in this article, $n = 1, 2, 3, 4, 5, 6, \dots$ but not too large relative to a considered genomic sequence).

The second Chargaff's rule about approximate equalities of pyrimidines and purines ($\%A \approx \%T$ and $\%C \approx \%G$) in any long DNA nucleotide sequence (that is in any long DNA n-text under $n = 1$) is a particular case of this general rule for n-texts.

And what one can say about equalities of percentage sums inside pairs of matrix rows, which are enumerated by binary-inversible numbers and contain percents of corresponding n-plets in n-texts of genomic DNA? The revealed phenomenological rule is that both such rows also have practically the same percentage sums. Figs. 4.4-4.6 show examples of performance of this rule for rows of the probability matrices in Figs. 1.1-1.4.

Rows	Percentage sums in rows
11	$0.05409+0.07274+0.05033+0.09504 = \mathbf{0.27219}$
00	$0.09568+0.07286+0.05046+0.05419 = \mathbf{0.27319}$
10	$0.07134+0.01031+0.07429+0.07137 = \mathbf{0.22730}$
01	$0.06008+0.06312+0.04402+0.06008 = \mathbf{0.22731}$

Fig. 4.4. Percentage sums in rows of the probability matrix of 16 doublets from Fig. 1.2.

Bold boxes mark pairs of rows enumerated with binary-inversible numbers shown at the left. In each of the boxes, percentage sums in both rows are practically the same.

Rows	Percentage sums in rows
111	$0.01385+0.01878+0.01524+0.01861+0.01183+0.01977+0.01447+0.03693 = \mathbf{0.14946}$
000	$0.03725+0.01884+0.01988+0.01895+0.01445+0.01534+0.01185+0.01382 = \mathbf{0.15039}$
110	$0.01853+0.00291+0.01789+0.02104+0.01622+0.00254+0.02375+0.01988 = \mathbf{0.12275}$
001	$0.01972+0.01981+0.01457+0.01947+0.00956+0.01115+0.01256+0.01600 = \mathbf{0.12285}$
101	$0.01758+0.01275+0.00251+0.00227+0.01317+0.01942+0.01441+0.02237 = \mathbf{0.10448}$
010	$0.02226+0.00233+0.01939+0.01284+0.01437+0.00253+0.01327+0.01756 = \mathbf{0.10456}$
100	$0.02009+0.02088+0.00259+0.00291+0.02388+0.01781+0.01614+0.01848 = \mathbf{0.12277}$
011	$0.01588+0.01964+0.01103+0.01986+0.01255+0.01456+0.00962+0.01960 = \mathbf{0.12273}$

Fig. 4.5. Percentage sums in rows of the probability matrix of 64 triplets from Fig. 1.3.

Bold boxes mark pairs of rows enumerated with binary-inversible numbers shown at the left. In each of the boxes, percentage sums in both rows are practically the same.

Rows	Percentage sums in rows
------	-------------------------

1111	0.0033+0.0055+0.0042+0.0044+0.0040+0.0056+0.0032+0.0070+ 0.0030+0.0042+0.0040+0.0053+0.0032+0.0059+0.0055+0.0149 = 0.0830
0000	0.0150+0.0072+0.0055+0.0045+0.0059+0.0057+0.0043+0.0054+ 0.0055+0.0032+0.0040+0.0042+0.0032+0.0039+0.0030+0.0033 = 0.0838
1110	0.0041+0.0010+0.0044+0.0058+0.0047+0.0010+0.0040+0.0044+ 0.0041+0.0005+0.0051+0.0054+0.0047+0.0006+0.0095+0.0071 = 0.0664
0001	0.0073+0.0078+0.0038+0.0051+0.0037+0.0046+0.0042+0.0051+ 0.0030+0.0028+0.0029+0.0042+0.0023+0.0024+0.0030+0.0046 = 0.0666
1101	0.0050+0.0029+0.0008+0.0006+0.0036+0.0039+0.0049+0.0059+ 0.0037+0.0032+0.0006+0.0006+0.0040+0.0070+0.0037+0.0066 = 0.0569
0010	0.0077+0.0006+0.0063+0.0038+0.0049+0.0006+0.0045+0.0057+ 0.0038+0.0004+0.0032+0.0027+0.0042+0.0010+0.0034+0.0052 = 0.0580
1100	0.0048+0.0058+0.0006+0.0009+0.0057+0.0047+0.0045+0.0058+ 0.0049+0.0044+0.0007+0.0007+0.0071+0.0057+0.0049+0.0047 = 0.0659
0011	0.0051+0.0063+0.0034+0.0063+0.0041+0.0049+0.0031+0.0061+ 0.0023+0.0031+0.0017+0.0035+0.0031+0.0042+0.0023+0.0052 = 0.0648
1011	0.0052+0.0057+0.0027+0.0038+0.0010+0.0006+0.0003+0.0006+ 0.0033+0.0045+0.0032+0.0063+0.0042+0.0049+0.0039+0.0078 = 0.0579
0100	0.0068+0.0058+0.0006+0.0006+0.0070+0.0039+0.0032+0.0029+ 0.0037+0.0048+0.0006+0.0008+0.0041+0.0036+0.0036+0.0051 = 0.0570
1010	0.0058+0.0009+0.0035+0.0028+0.0007+0.0003+0.0005+0.0008+ 0.0049+0.0005+0.0064+0.0035+0.0046+0.0007+0.0049+0.0059 = 0.0466
0101	0.0057+0.0040+0.0005+0.0006+0.0030+0.0055+0.0026+0.0041+ 0.0032+0.0027+0.0006+0.0005+0.0025+0.0031+0.0032+0.0057 = 0.0476
1001	0.0048+0.0036+0.0046+0.0051+0.0005+0.0004+0.0008+0.0006+ 0.0047+0.0056+0.0033+0.0050+0.0031+0.0037+0.0047+0.0057 = 0.0563
0110	0.0057+0.0006+0.0051+0.0052+0.0037+0.0004+0.0056+0.0036+ 0.0047+0.0008+0.0033+0.0046+0.0030+0.0005+0.0046+0.0048 = 0.0563
1000	0.0073+0.0044+0.0053+0.0058+0.0006+0.0010+0.0005+0.0010+ 0.0096+0.0040+0.0051+0.0044+0.0046+0.0047+0.0040+0.0041 = 0.0666
0111	0.0046+0.0049+0.0042+0.0051+0.0024+0.0045+0.0028+0.0078+ 0.0030+0.0041+0.0029+0.0038+0.0023+0.0037+0.0029+0.0073 = 0.0664

Fig. 4.6. Percentage sums in rows of the probability matrix of 256 tetraplets from Fig. 1.4.

Bold boxes mark pairs of rows enumerated with binary-inversible numbers shown at the left. In each of the boxes, percentage sums in both rows are practically the same.

One should remind that binary numeration of rows uses the following denotations as it was above-explained in the Introduction: the binary symbol **1** denotes amino molecules (C and A) and the binary symbol **0** denotes keto molecules (T and G). Correspondingly, each of the rows of any such matrices (like in Figs. 1.1-1.4) contains all n-plets having an identical sequence of amino and keto molecules. For example, in the matrix of 64 triplets in Fig. 1.3, the column with its binary numeration **011** contains all triplets with the identical sequence “**keto-amino-amino**”: TCC, TCA, TAC, TAA, GCC, GCA, GAC, GAA. The row having the binary-inverse numeration **100** contains all 8 triplets with the sequence of opposite type “**amino-keto-keto**”: CTT, CTG, CGT, CGG, ATT, ATG, AGT, AGG. Each of the triplets of the first sequence is transformed into an appropriate triplet of the second sequence by the following simultaneous replacements: C↔T, G↔A. We term such pairs of sequences as “complementary sequences” relative to indicators “amino-or-keto”.

The described phenomenological facts, whose separate examples are represented in Figs. 4.4-4.6 about the equalities of total percentage sums of all n-plets in the noted subsets based on the indicators “amino-or-keto”, can be expressed by the following rule, which is a candidacy for a role of the universal genetic rule:

- In any n-text of DNA of eukaryotic and prokaryotic genomes, a total percentage sum of all those n-plets, whose contents are identical to each other relative to some sequence of amino and keto, is approximately equal to a total percentage sum of all those n-plets, whose contents are identical to each other relative to the complementary sequence of keto and amino (although the individual percentages of the corresponding n-plets in the considered complementary sequences can differ significantly from each other, as can be seen from Figs. 4.4-4.6).

Both of these probability rules (for the columns and the rows), which are formulated in this section, holds also for n-texts in epi-chains of different genomic DNA, that is, for regular sparsed DNA sequences. The notion "DNA epi-chains" was introduced in [Petoukhov, 2019a, 2020a-c]. By definition, in a nucleotide sequence of any DNA strand N_1 with sequentially numbered nucleotides 1, 2, 3, 4, ..., epi-chains of different orders k are such subsequences that contain only those nucleotides, whose numeration differ from each other by natural number $k = 1, 2, 3, 4, \dots$. For example, in any single-stranded DNA, one can consider its epi-chain of the second-order N_2 , in which its nucleotide sequence numbers differ by $k = 2$: an epi-chain N_2 contains nucleotides with numerations 1, 3, 5, By analogy, an epi-chain of the third-order N_3 is connected with $k = 3$ and contains a subsequence of nucleotides with numerations 1, 4, 7, 10, ..., and so on.

5. The symmetry of percentages of mirror-complemented n-plets in n-texts of genomic DNA

This section is devoted to the symmetry principle related to pairs of mirror-complemented n-plets in single-stranded DNA. It is such two n-plets, which is identical if one of them is read in the opposite order with simultaneous replacement of each nucleotide in its content by complemented nucleotide ($A \leftrightarrow T, C \leftrightarrow G$). For example, the triplet ACG is mirror-complemented to the triplet CGT (but not to TGC).

The work [Prahbu, 1993] showed the existence of the following symmetry principle in long DNA. In any long DNA sequence of nucleotides (more than 50 000 nucleotides), one can take an arbitrary kind of n-plets ($n = 2, 3, 4, 5, 6$) and then calculates the total quantity of all such n-plets (including n-plets overlapping each other). It occurs that this DNA contains also approximately an equal quantity of mirror-complemented n-plets (including all mirror-complemented n-plets overlapping each other).

In our research, we initiatively study DNA n-texts (under $n=2, 3, 4, \dots$), which were not considered at all by other authors till now. One should note that each of the n-texts has no overlapping of its n-plets, which are separated from each other.

Have such n-texts in genomic DNA (and also in enough long DNA sequences in general) similar symmetry principle related to pairs of mirror-complemented n-plets? Yes, our study confirms the existence of a similar symmetry principle in single-stranded DNA sequences of eukaryotic and prokaryotic genomes. Figs. 5.1, 5.2 show some examples of this symmetry principle n-plets of the single-stranded DNA of the human chromosome №1 using the above-presented percentage data from Figs. 1.2-1.4. Those n-plets, which coincide with their mirror-complemented ones (CG, AT, GC, TA), are not shown.

% in doublet 1	% in doublet 2	% in doublet 1	% in doublet 2
%CC = 0.05409	%GG = 0.05419	%AC = 0.05033	%GT = 0.05046
%CA = 0.07274	%TG = 0.07286	%AA = 0.09504	%TT = 0.09568
%CT = 0.07134	%AG = 0.07137	%TC = 0.06008	%GA = 0.06008

Fig. 5.1. Percentages of mirror-complemented doublets, whose corresponding pairs are presented inside bold boxes, in the 2-text of the DNA of human chromosome №1. All values of percent are taken from Fig. 1.2.

% triplet 1	% triplet 2	% triplet 1	% triplet 2
%CCC = 0.01385	%GGG = 0.01382	%ACC = 0.01183	%GGT = 0.01185

%CCA = 0.01878	%TGG = 0.01895	%ACA = 0.01977	%TGT = 0.01988
%CCT = 0.01853	%AGG = 0.01848	%ACT = 0.01622	%AGT = 0.01614
%CCG = 0.00291	%CGG = 0.00291	%ACG = 0.00254	%CGT = 0.00259
%CAC = 0.01524	%GTG = 0.01534	%AAT = 0.02375	%ATT = 0.02388
%CAA = 0.01861	%TTG = 0.01884	%AAA = 0.03693	%TTT = 0.03725
%CAT = 0.01789	%ATG = 0.01781	%AAC = 0.01447	%GTT = 0.01445
%CTC = 0.01758	%GAG = 0.01756	%ATC = 0.01317	%GAT = 0.01327
%CTA = 0.01275	%TAG = 0.01284	%ATA = 0.01942	%TAT = 0.01939
%CGC = 0.00251	%GCG = 0.00253	%AGC = 0.01441	%GCT = 0.01437
%CGA = 0.00227	%TCG = 0.00233	%AAG = 0.01988	%CTT = 0.02009
%TCC = 0.01588	%GGA = 0.01600	%AGA = 0.02237	%TCT = 0.02226
%TCA = 0.01964	%TGA = 0.01947	%GCC = 0.01255	%GGC = 0.01256
%TAC = 0.01103	%GTA = 0.01115	%GCA = 0.01456	%TGC = 0.01457
%TAA = 0.01986	%TTA = 0.01981	%GAC = 0.00962	%GTC = 0.00956
%CAG = 0.02104	%CTG = 0.02088	%GAA = 0.01960	%TTC = 0.01972

Fig. 5.2. Percentages of mirror-complemented triplets, whose corresponding pairs are presented inside bold boxes, in the 3-text of the DNA of human chromosome №1. All values of percent are taken from Fig. 1.3.

Using Fig. 1.4, one can check that the same symmetry principle holds also for percentages of mirror-complemented tetraplets in the 4-text of this chromosomal DNA.

The described symmetry principle for percentages of mirror-complemented n-plets in single-stranded DNA of eukaryotic and prokaryotic genomes shows additionally that the system of probabilities in n-texts of genomic DNA molecules has many special interconnections among probabilities of its members. Briefly speaking, a stochastic organization of genomes is a special kind of very limited stochastics.

6. Some additions to algebra-holographic principles in the genetic system.

Living organisms possess genetically inherited physiological properties, which seem to be analogical to properties of holography with its non-local record of information. In particular, the concept of the connection of brain functions with the properties of holography is widely known, presented in Pribram's book "Languages of the Brain" [Pribram, 1971]. This book emphasizes that holographic description is unmatched for explaining problems of perception, especially problems of image formation and fantastic ability to recognize.

Numerous known data about holographic-like features in inherited physiological systems provoke an idea about a connection of the genetic system with algebra-holographic formalisms. This idea about algebra-holographic principles in genetics is under systematic development by the author. The first results and thoughts are described in detail in the previous author's work [Petoukhov, 2021b, section 16]. Now this section presents some essential additions to this previous work, from which the following materials about the bit-reversal holography in genetics should be briefly reminded, including binary-oppositional features of the matrices of DNA alphabets of n-plets and also the method of bit-reversal permutations.

As it is known, the set of 64 triplets, according to their features of coding 20 amino acids, is divided into two subsets of 32 triplets in each [Rumer, 1968; Fimmel, Strüngmann, 2016; Petoukhov, 2008]:

- 32 triplets with "strong roots" (that is, with 8 doublets CC, CT, CG, AC, TC, GC, GT, GG at the beginning of triplets), whose code meanings do not depend on the letter in their third position;
- 32 triplets with "weak roots" (that is, with the remaining 8 doublets CA, AA, AT, AG, TA, TT, TG, GA at the beginning of triplets), whose code meanings depend on the letter in their third position.

Fig. 6.1 shows the beginning of the tensor family of matrices $[C, A; T, G]^{(n)}$ under $n = 2, 3, 4$, which represent the alphabets of 16 doublets, 64 triplets, and 256 tetraplets. The mentioned strong doublets

and also triplets and tetraplets with strong roots are marked by black color in symbolic matrices in Fig. 6.1 by contrast to other n-plets having weak roots.

	11	10	01	00
11	CC	CA	AC	AA
10	CT	CG	AT	AG
01	TC	TA	GC	GA
00	TT	TG	GT	GG

	111	110	101	100	011	010	001	000
111	CCC	CCA	CAC	CAA	ACC	ACA	AAC	AAA
110	CCT	CCG	CAT	CAG	ACT	ACG	AAT	AAG
101	CTC	CTA	CGC	CGA	ATC	ATA	AGC	AGA
100	CTT	CTG	CGT	CGG	ATT	ATG	AGT	AGG
011	TCC	TCA	TAC	TAA	GCC	GCA	GAC	GAA
010	TCT	TCG	TAT	TAG	GCT	GCG	GAT	GAG
001	TTC	TTA	TGC	TGA	GTC	GTA	GGC	GGA
000	TTT	TTG	TGT	TGG	GTT	GTG	GGT	GGG

=

	1111	1110	1101	1100	1011	1010	1001	1000	0111	0110	0101	0100	0011	0010	0001	0000
1111	CCCC	CCCA	CCAC	CCAA	CACC	CACA	CAAC	CAAA	ACCC	ACCA	ACAC	ACAA	AACC	AACA	AAAC	AAAA
1110	CCCT	CCCG	CCAT	CCAG	CACT	CACG	CAAT	CAAG	ACCT	ACCG	ACAT	ACAG	AACT	AACG	AAAT	AAAG
1101	CCTC	CCTA	CCGC	CCGA	CATC	CATA	CAGC	CAGA	ACTC	ACTA	ACGC	ACGA	AATC	AATA	AAGC	AAGA
1100	CCTT	CCTG	CCGT	CCGG	CATT	CATG	CAGT	CAGG	ACTT	ACTG	ACGT	ACGG	AATT	AATG	AAGT	AAGG
1011	CTCC	CTCA	CTAC	CTAA	CGCC	CGCA	CGAC	CGAA	ATCC	ATCA	ATAC	ATAA	AGCC	AGCA	AGAC	AGAA
1010	CTCT	CTCG	CTAT	CTAG	CGCT	CGCG	CGAT	CGAG	ATCT	ATCG	ATAT	ATAG	AGCT	AGCG	AGAT	AGAG
1001	CTTC	CTTA	CTGC	CTGA	CGTC	CGTA	CGGC	CGGA	ATTC	ATTA	ATGC	ATGA	AGTC	AGTA	AGGC	AGGA
1000	CTTT	CTTG	CTGT	CTGG	CGTT	CGTG	CGGT	CGGG	ATTT	ATTG	ATGT	ATGG	AGTT	AGTG	AGGT	AGGG
0111	TCCC	TCCA	TCAC	TCAA	TACC	TACA	TAAC	TAAA	GCCC	GCCA	GCAC	GCAA	GACC	GACA	GAAC	GAAA
0110	TCCT	TCCG	TCAT	TCAG	TACT	TACG	TAAT	TAAG	GCCT	GCCG	GCAT	GCAG	GACT	GACG	GAAT	GAAG
0101	TCTC	TCTA	TCGC	TCGA	TATC	TATA	TAGC	TAGA	GCTC	GCTA	GCGC	GCGA	GATC	GATA	GAGC	GAGA
0100	TCTT	TCTG	TCGT	TCGG	TATT	TATG	TAGT	TAGG	GCTT	GCTG	GCGT	GCGG	GATT	GATG	GAGT	GAGG
0011	TTCC	TTCA	TTAC	TTAA	TGCC	TGCA	TGAC	TGAA	GTCC	GTCA	GTAC	GTAA	GGCC	GGCA	GGAC	GGAA
0010	TTCT	TTCG	TTAT	TTAG	TGCT	TGCG	TGAT	TGAG	GTCT	GTCC	GTAT	GTAG	GGCT	GGCG	GGAT	GGAG
0001	TTTC	TTTA	TTGC	TTGA	TGTC	TGTA	TGGC	TGGA	GTTC	GTTA	GTGC	GTGA	GGTC	GGTA	GGGC	GGGA
0000	TTTT	TTTG	TTGT	TTGG	TGTT	TGTG	TGGT	TGGG	GTTT	GTTG	GTGT	GTGG	GGTT	GGTG	GGGT	GGGG

Fig. 6.1. Rooted mosaic matrices $[C, A; T, G]^{(2)}$, $[C, A; T, G]^{(3)}$, and $[C, A; T, G]^{(4)}$ for DNA alphabets of 16 doublets, 64 triplets, and 256 tetraplets. Black color denotes 8 strong doublets and also 32 triplets and 128 tetraplets with strong roots.

It should be additionally noted that cooperative percentage organization of n-texts of genomic DNA sequences is connected with this structural division of the n-plets alphabets into equal sub-alphabets of n-plets with strong roots and weak roots and also with meander patterns of Rademacher functions in rows of the genetic matrices in Fig. 6.1 (see details in [Petoukhov, 2021b, section 15]). For this reason, the stochastic system of percentages of n-plets in n-texts of DNA molecules in genomes has additional interconnections of its members and obeys appropriate limitations. Meander patterns of Rademacher functions exists also in many mosaic $(2^n \times 2^n)$ -matrices, which represent probability rules using four kinds of card symbols in [Petoukhov, 2021b, Figs. 7.9-7.12, 8.3, 8.4, 9.1-9.7]. The author believes that such systematic existence of meander patterns of Rademacher functions in structured genetic matrices is not accidental at all and it is connected with the known fact about relations of Rademacher functions to the probability theory and binary expansions of real numbers t , $0 \leq t \leq 1$.

In digital signal processing, the method of bit-reversal permutations of the binary numbering of columns and rows in square matrices, which sometimes is termed bit-reversal holography, plays an important role; the method is connected, in particularly, noise-immunity coding and algorithms of fast Fourier transform [Gold and Rader, 1969; Karp, 1996; Lyons, 2010; Shiman, Patsey, 2013; Shishmintsev, 2012; Yang et al., 2013]. This method is based on a backward order of reading of binary numbering of columns and rows (001 becomes 100, etc.) in the square $(2^n \times 2^n)$ -matrices with appropriate permutations of columns and rows. For example, under bit-reversal permutations, the

binary-numeric sequence 111, 110, 101, 100, 011, 010, 001, 000 (its decimal analog is the sequence 7, 6, 5, 4, 3, 2, 1) is transformed to the binary sequence 111, 011, 101, 001, 110, 010, 100, 000 (its decimal analog is 7, 3, 5, 1, 6, 2, 4, 0, where all odd numbers are collected inside the left half of the sequence and all even numbers – in the right half). Such renumbering of the columns and rows of the matrix, having some internal image, leads to a corresponding permutation of its cells and the appearance of a new matrix with a new image. If a part of the image in this new matrix is removed then the repeated backward reading of binary numerations of its columns and rows restore the original image largely since all introduced defects occur to be dispersed and do not interfere with the recognition of the original image (see examples in [Petoukhov, 2021b, section 16]).

The author's application of the holographic method of bit-reversal permutations to alphabetic mosaic matrices from their tensor family $[C, A; T, G]^{(n)}$, whose first members are shown above in Fig. 6.1, has given interesting results illustrated by Fig. 6.2.

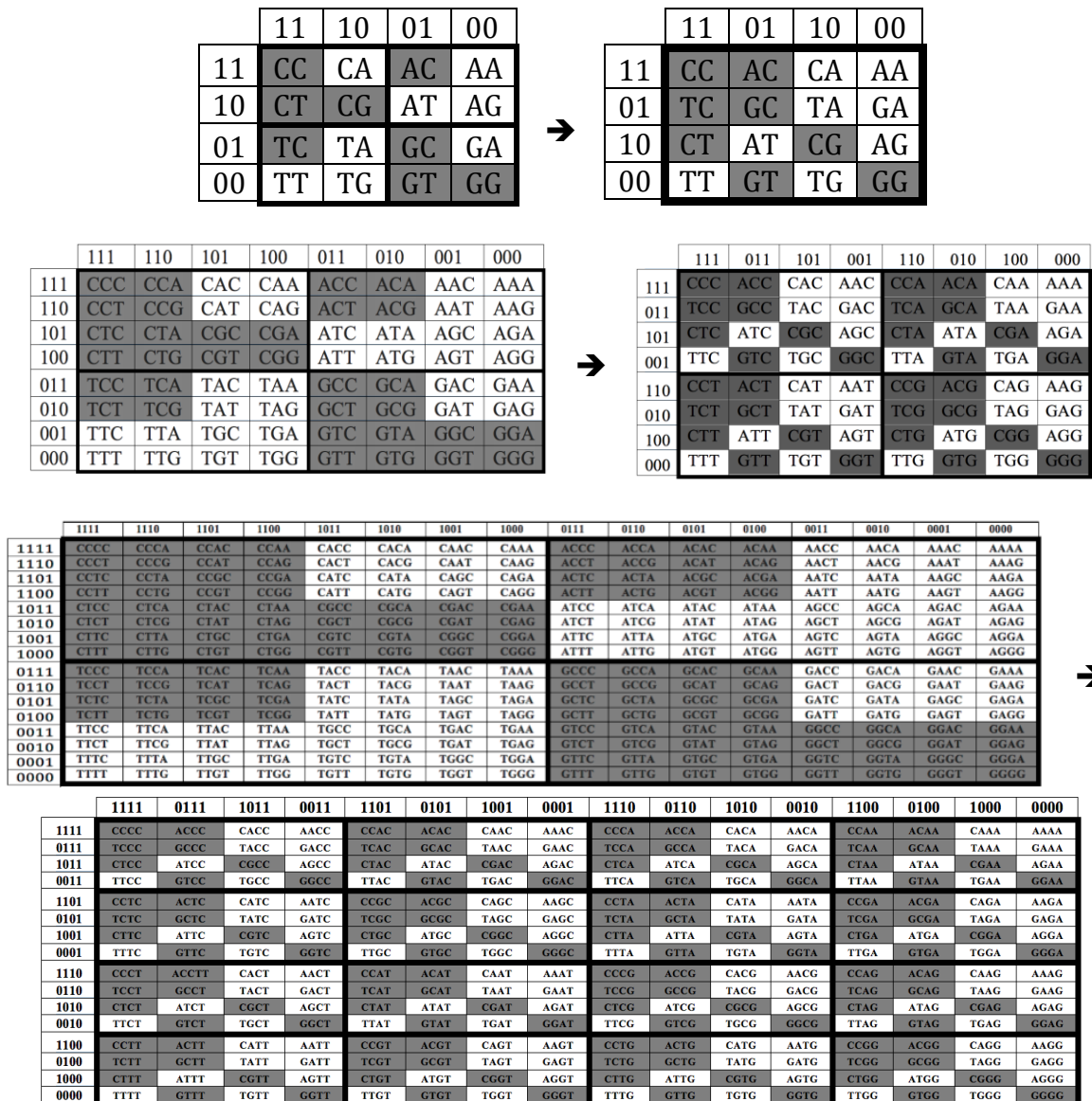


Fig. 6.2. Transformations of the alphabetic mosaic matrices $[C, A; T, G]^{(n)}$ from Fig. 6.1 into new alphabetic mosaic matrices $[C, A; T, G]^{(n)}$ _{bit-reversal} by the method of bit-reversal permutations inside binary numeration of their columns and rows.

The first interesting result of such bit-reversal transformations of genetic matrices from the tensor family $[C, A; T, G]^{(n)}$ is that all received mosaic matrices $[C, A; T, G]^{(n)}$ _{bit-reversal} under $n = 3, 4, \dots$ (Fig. 16.1.3) are block matrices: the family of their mosaics is tensor colonies or crystal-like unions of the same mosaic (4*4)-block representing the bit-reversal mosaic (4*4)-matrix of the DNA alphabet of

doublets (Fig. 6.2, on the right in the top row). This fact additionally emphasizes an algebraic nature of the system of structured DNA and RNA alphabets and its close connection with the bit-reversal holography. The author conditionally terms these matrix crystal-like colonies of the same mosaic (4*4)-block as “matrix crystals” of DNA- and RNA- alphabets of n -plets. The alphabetical matrix crystals can be briefly termed α -crystals (using that α is the first letter of the Greek alphabet and that the Latin letter A and the Cyrillic A, which are the first letters in corresponding alphabets, were originated from the letter α). Fig. 6.3 illustrates this mosaic block interrelation of bit-reversed matrices of many DNA-alphabets of n -plets in the numeric form. The numeric (4*4)-matrix [1, 1, -1, -1; 1, 1, -1, -1; 1, -1, 1, -1; -1, 1, -1, 1], which plays a role of general cell in the numeric matrix crystals in Fig. 6.3, we term α -matrix.

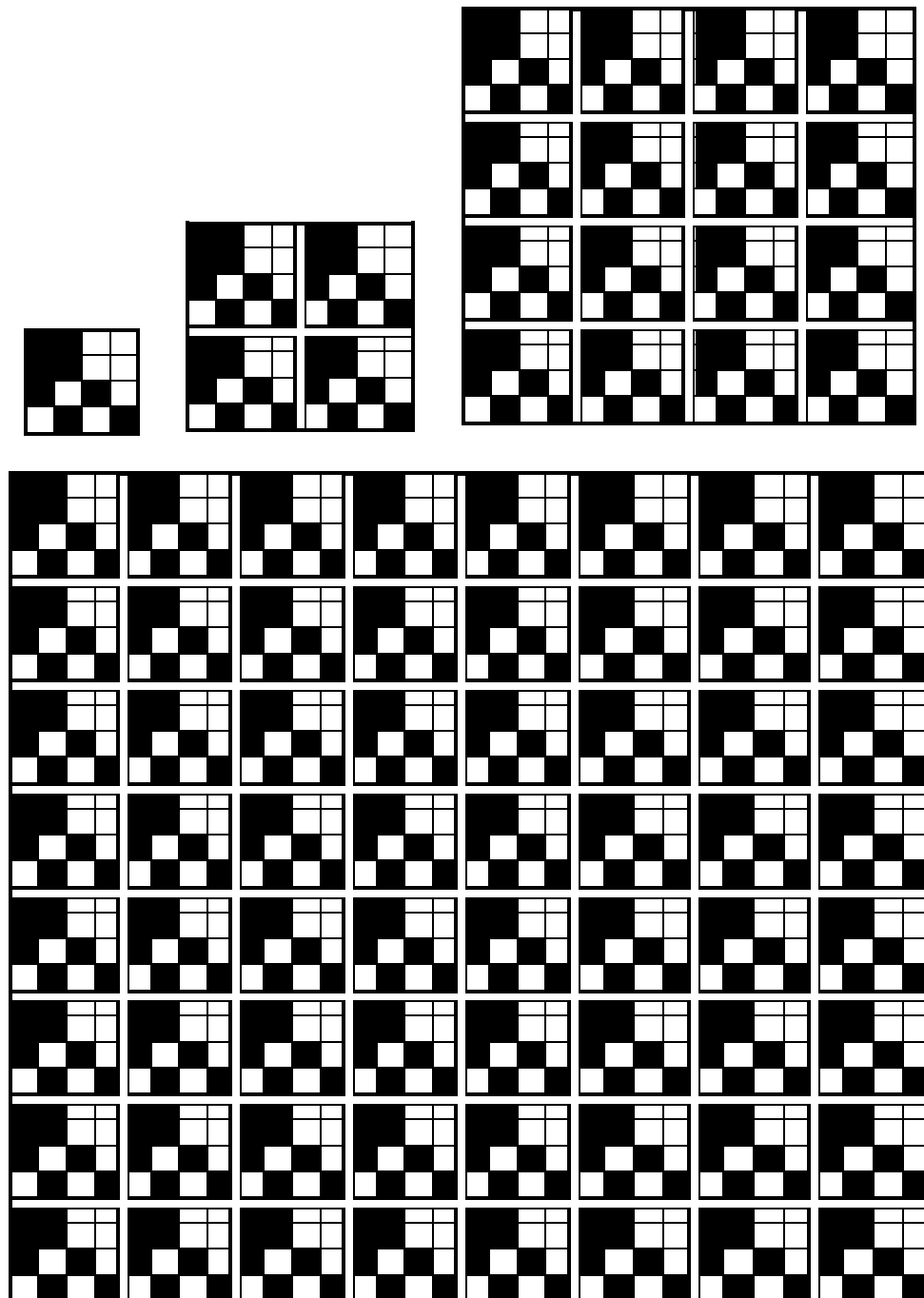


Fig. 6.3. “Matrix crystals” representing in the numeric form the interrelated mosaics of symbolic matrices $[C, A; T, G]^{(n)}$ bit-reversal of DNA-RNA alphabets from Fig. 6.2. In the numeric matrices, each of the black cells contains “+1” and each of the white cells contains “-1”. The shown multi-block matrices are colonies or unions of the same numeric (4*4)-matrix (α -matrix) representing the symbolic matrix $[C, A; T, G]^{(2)}$ bit-reversal of the alphabet of 16 doublets.

Each of the numeric matrices in Fig. 6.3 can be constructed from the α -matrix (denoted below as α) by the algorithm (6.1) based on its tensor product with the matrix $[1, 1; 1, 1]$:

$$[1, 1; 1, 1]^{(n)} \otimes \alpha = [1, 1; 1, 1]^{(n)} \otimes [1, 1, -1, -1; 1, 1, -1, -1; 1, -1, 1, -1; -1, 1, -1, 1] \quad (6.1)$$

The matrix $[1, 1; 1, 1]$ used in (6.1) is the matrix representation of a 2-dimensional hyperbolic number with unit coordinates. Deep structural connections of genetic informatics with 2^n -dimensional hyperbolic numbers are described in [Petoukhov, 2019b, 2021c].

The second interesting result of the described bit-reversal transformations of genetic matrices of the tensor family $[C, A; T, G]^{(n)}$ is the following. The α -matrix, which is algorithmically repeated in the matrix crystals in Fig. 6.3, is a sum of 4 sparse matrices, whose set is closed relative to multiplication and defines the multiplication table of base elements of the known algebra of 4-dimensional split-quaternions introduced by J. Cockle in 1849 (Fig. 6.4). In particular, split-quaternions are used in hyperbolic geometry for describing hyperbolic motions in the Poincare disk model [Karzel, Kist, 1985; <https://en.wikipedia.org/wiki/Split-quaternion>].

$$\alpha = \begin{vmatrix} 1, & 1, & -1, & -1 \\ 1, & 1, & -1, & -1 \\ 1, & -1, & 1, & -1 \\ -1, & 1, & -1, & 1 \end{vmatrix} = \begin{vmatrix} 1,0,0,0 \\ 0,1,0,0 \\ 0,0,1,0 \\ 0,0,0,1 \end{vmatrix} + \begin{vmatrix} 0,0,-1,0 \\ 0,0,0,-1 \\ 1,0,0,0 \\ 0,1,0,0 \end{vmatrix} + \begin{vmatrix} 0,0,0,-1 \\ 0,0,-1,0 \\ 0,-1,0,0 \\ -1,0,0,0 \end{vmatrix} + \begin{vmatrix} 0,1,0,0 \\ 1,0,0,0 \\ 0,0,0,-1 \\ 0,0,-1,0 \end{vmatrix} = j_0 + j_1 + j_2 + j_3$$

*	j_0	j_1	j_2	j_3
j_0	j_0	j_1	j_2	j_3
j_1	j_1	$-j_0$	j_3	$-j_2$
j_2	j_2	$-j_3$	j_0	$-j_1$
j_3	j_3	j_2	j_1	j_0

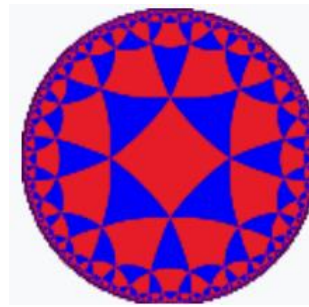
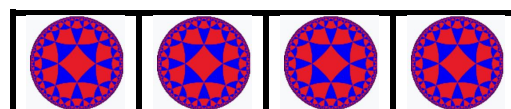


Fig. 6.4. The decomposition of the α -matrix gives 4 sparse matrices ($\alpha = j_0 + j_1 + j_2 + j_3$) whose set is closed relative to multiplication (top row) and corresponds to the multiplication table of split-quaternions by J.Cockle. One of the possible graphical symbols of the Poincare disk model of Lobachevsky hyperbolic geometry is also shown here to remind about using split-quaternions for describing hyperbolic motions in this model (the symbol is reproduced from https://commons.wikimedia.org/wiki/File:Uniform_tiling_433-t0.png in accordance with the Creative Commons CC0 License allowing such reproduction).

If each of the repeated α -matrices in the multi-block matrices in Fig. 16.1.4 is replaced by the shown symbol of the Poincare disk model, the artistic representations of these matrices appear whose examples are given in Fig. 6.5. Such artistic representations are useful for developing geometric intuition.



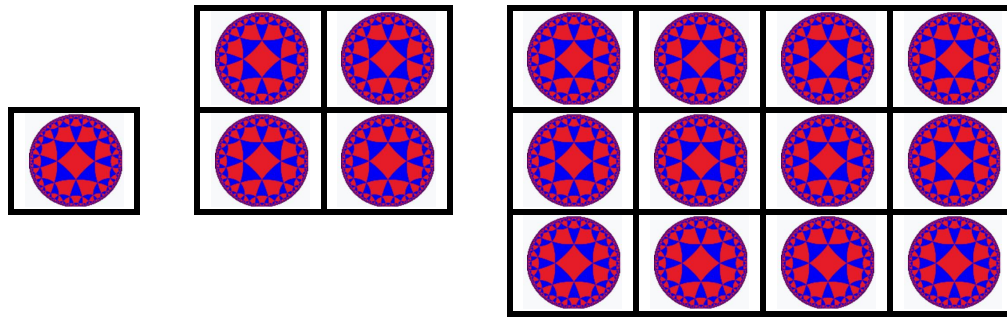


Fig. 6.5. Examples of the artistic representations of genetic multi-block matrices from Fig. 6.3 are received by replacements of their blocks (α -matrices) with the symbol of the Poincaré disk model (from [Petoukhov, 2021b]). This symbol is reproduced from https://commons.wikimedia.org/wiki/File:Uniform_tiling_433-t0.png in accordance with the Creative Commons CC0 License allowing such reproduction. Combinations of symbols into multi-block constructions are made by the author.

The presented study of the algebraic-holographic structures of multi-alphabetic genetic informatics unexpectedly reveals the structural parallels of genetic informatics with holographic quantum codes and algebraic-holographic principles, actively developed in modern theoretical physics by many famous authors. To illustrate these parallels, let us use excerpts from works on holographic quantum error-correcting codes [Pastawski et al., 2015; Preskill, 2016]. The Poincaré disk model and the corresponding hyperbolic space tilings are used in these works. Fig. 6.6, which is taken from these works, briefly illustrates these parallels by using the same symbol of the Poincaré disk model, which is presented above in connection with the algebraic-holographic tensor properties of genetic informatics in Figs. 6.4 and 6.5.

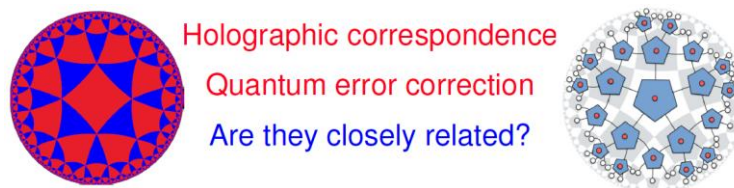


Fig. 6.6. The illustration to the theme of holographic quantum error-correcting codes (from [Preskill, 2016] in accordance with a personal permission by its author J.Preskill).

The following quotes from these works, which describe quantum error-correcting codes with a tensor network structure, clarify these parallels in more detail. *“The tensor network is supported on a uniform tiling of a hyperbolic space, known as a hyperbolic tessellation. ... We shall focus on examples based on tilings of two-dimensional hyperbolic space, which are specific realizations of uniform hyperbolic tilings known as hyperbolic tessellations”* [Pastawski et al., 2015]. *«Holographic quantum error-correcting codes are constructed by contracting perfect tensors according to a tiling of hyperbolic space by polygons»* [Preskill, 2016].

Let us return to the family of genetic mosaic matrices $[C, A; T, G]^{(n)}_{\text{bit-reversal}}$ (Fig. 6.2), which were received by the algebra-holographic method, to study the following question about the genetic code of amino acids: how 20 amino acids and stop-codons, which are encoded by 64 triplets, are located in the bit-reversal (8×8) -matrix $[C, A; T, G]^{(3)}_{\text{bit-reversal}}$? Does their arrangement have a pronounced law character, which can additionally confirm the deep consistency of the amino acid genetic coding system with the holographic method of bit-reverse permutations, which led to this matrix?

Fig. 6.7 shows interrelated locations of triplets, amino acids, and stop-codons in the bit-reversal (8×8) -matrix $[C, A; T, G]^{(3)}_{\text{bit-reversal}}$ (from Fig. 6.2) for the case of the Vertebrate Mitochondrial Code, which is the most symmetrical among known dialects on the genetic code and which is called in genetics the most ancient and "ideal" [Frank-Kamenetskii, 1988] (other dialects of the genetic code have small

differences from this basic one). It can be seen from Fig. 6.7 that the upper and lower halves of the matrix $[C, A; T, G]^{(3)\text{bit-reversal}}$ are unexpectedly identical to each other in the composition and arrangement of amino acids and stop-codons. All so-termed high-degenerate amino acids (Pro, Thr, Ser, Ala, Leu, Arg, Val, Gly), which are encoded by triplets with strong roots (black cells), are located in 4 quadrants identically. These strict regularities give additional pieces of evidence that genetic informatics is closely connected with principles of algebraic holography.

CCC Pro	ACC Thr	CAC His	AAC Asn	CCA Pro	ACA Thr	CAA Gln	AAA Lys
UCC Ser	GCC Ala	UAC Tyr	GAC Asp	UCA Ser	GCA Ala	UAA Stop	GAA Glu
CUC Leu	AUC Ile	CGC Arg	AGC Ser	CUA Leu	AUA Met	CGA Arg	AGA Stop
UUC Phe	GUC Val	UGC Cys	GGC Gly	UUA Leu	GUA Val	UGA Trp	GGA Gly
CCU Pro	ACU Thr	CAU His	AAU Asn	CCG Pro	ACG Thr	CAG Gln	AAG Lys
UCU Ser	GCU Ala	UAU Tyr	GAU Asp	UCG Ser	GCG Ala	UAG Stop	GAG Glu
CUU Leu	AUU Ile	CGU Arg	AGU Ser	CUG Leu	AUG Met	CGG Arg	AGG Stop
UUU Phe	GUU Val	UGU Cys	GGU Gly	UUG Leu	GUG Val	UGG Trp	GGG Gly

Fig. 6.7. Arrangement of amino acids and stop-codons in the alphabetical matrix $[C, A; T, G]^{(3)\text{bit-reversal}}$ (from Fig. 6.2) of 64 triplets, which encode them (the case of the Vertebrate Mitochondria Code is presented).

Above in section 4, we showed that the genetic system is related to binary-inversible changes of binary numerations of n-plets. And what can one get by the simultaneous inversion ($1 \leftrightarrow 0$) of all binary symbols in binary numerations of columns and rows in the genetic matrices $[C, A; T, G]^{(n)\text{bit-reversal}}$ from Fig. 6.2? Such inversion rotates each of these mosaic matrices by 180 degrees. Fig. 6.8 shows such rotation transformation for the matrix $[C, A; T, G]^{(2)\text{bit-reversal}}$ of 16 doublets from Fig. 6.2.

	11	01	10	00							
11	CC	AC	CA	AA	→	00	GG	TG	GT	TT	
01	TC	GC	TA	GA		10	AG	CG	AT	CT	
10	CT	AT	CG	AG		01	GA	TA	GC	TC	
00	TT	GT	TG	GG		11	AA	CA	AC	CC	
					→	$\alpha_{\text{inverse}} =$	00	1	-1	1	-1
							10	-1	1	-1	1
							01	-1	-1	1	1
							11	-1	-1	1	1

Fig. 6.8. At left: the mosaic matrix $[C, A; T, G]^{(2)\text{bit-reversal}}$ of 16 doublets (at left) from Fig. 6.2. In middle: the result of its transformation by the inversion of all binary symbols ($1 \leftrightarrow 0$) inside binary numerations of its columns and rows. At right: this resulting matrix is numerically represented by the α_{inverse} -matrix, whose black (white) cells contain numbers «+1» («-1») (at right).

Similar rotation transformation of other matrices $[C, A; T, G]^n$ by 180 degrees generates new mosaic multi-block matrices whose black-and-white blocks are identical by their mosaic to the new (4*4)-matrix of 16 doublets in Fig. 6.8 on the right. If one represents each of the black (white) cells of these new matrices by number “+1” (“-1”) then new numeric “matrix crystals” arise, whose examples are shown in Fig. 6.9.

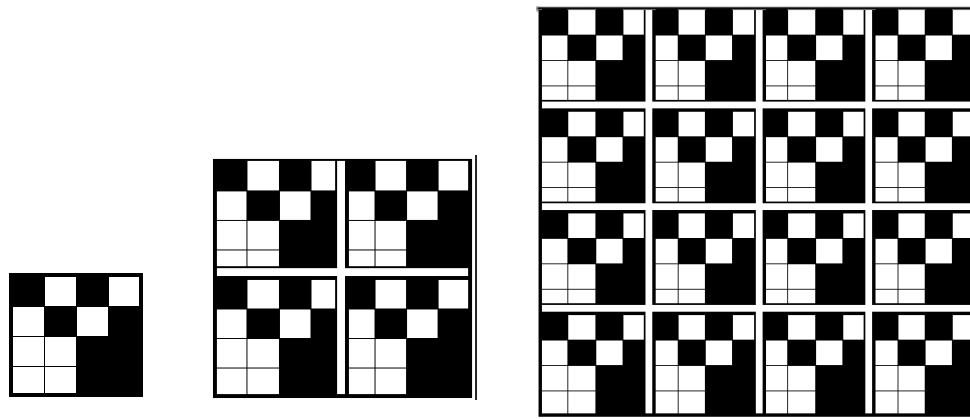


Fig. 6.9. Examples of new “matrix crystals” representing in the numeric form the interrelated mosaics of symbolic matrices, which arise in the result of the transformations of matrices $[C, A; T, G]^{(n)}$ bit-reversal from Fig. 6.2 by the inversion of all binary symbols ($1 \leftrightarrow 0$) inside binary numerations of their columns and rows. In the numeric matrices of these matrix crystals, each of the black (white) cells contains the number “+1” (“-1”). The shown multi-block matrices are colonies or aggregations of the α_{inverse} -matrix from Fig. 6.8.

It should be noted that this α_{inverse} -matrix is the sum of four new sparse matrices e_0, e_1, e_2, e_3 , shown in Fig. 6.10. But their set is also closed relative to multiplication and defines the same multiplication table of split-quaternions, which was shown in Fig. 6.4. It means that the α -matrix (Fig. 6.4) and the α_{inverse} -matrix are two different matrix representations of 4-dimensional split-quaternions with unit coordinates.

$$\alpha_{\text{inverse}} = \begin{vmatrix} 1, & -1, & 1, & -1 \\ -1, & 1, & -1, & 1 \\ -1, & -1, & 1, & 1 \\ -1, & -1, & 1, & 1 \end{vmatrix} = \begin{vmatrix} 1,0,0,0 \\ 0,1,0,0 \\ 0,0,1,0 \\ 0,0,0,1 \end{vmatrix} + \begin{vmatrix} 0, & 0, & 1, & 0 \\ 0, & 0, & 0, & 1 \\ -1, & 0, & 0, & 0 \\ 0, & -1, & 0, & 0 \end{vmatrix} + \begin{vmatrix} 0, & 0, & 0, & -1 \\ 0, & 0, & -1, & 0 \\ 0, & -1, & 0, & 0 \\ -1, & 0, & 0, & 0 \end{vmatrix} + \begin{vmatrix} 0, & -1, & 0, & 0 \\ -1, & 0, & 0, & 0 \\ 0, & 0, & 0, & 1 \\ 0, & 0, & 1, & 0 \end{vmatrix} = e_0 + e_1 + e_2 + e_3$$

*	e0	e1	e2	e3
e0	e0	e1	e2	e3
e1	e1	-e0	e3	-e2
e2	e2	-e3	e0	-e1
e3	e3	e2	e1	e0

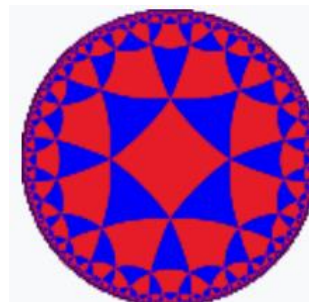


Fig. 6.10. The decomposition of the α_{inverse} -matrix gives 4 sparse matrices ($\alpha_{\text{inverse}} = e_0 + e_1 + e_2 + e_3$) whose set is closed relative to multiplication (top row) and corresponds to the multiplication table of split-quaternions. One of the possible graphical symbols of the Poincaré disk model of Lobachevsky hyperbolic geometry is also shown here to remind about using split-quaternions for describing hyperbolic motions in this model. This symbol is reproduced from https://commons.wikimedia.org/wiki/File:Uniform_tiling_433-t0.png in accordance with the Creative Commons CC0 License allowing such reproduction).

In art, the images of the Poincaré disk model are widely known thanks to Escher's graphics (Fig. 6.11).

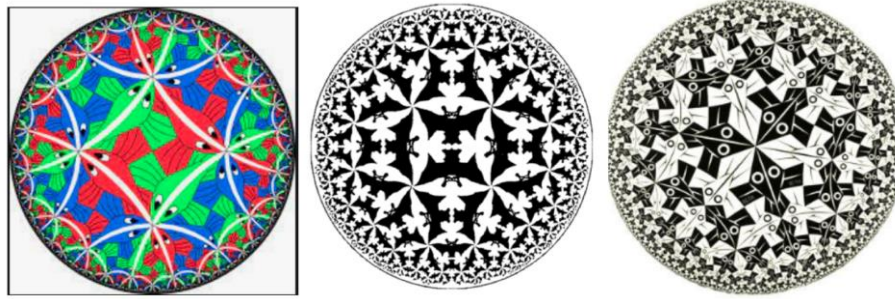


Fig. 6.11. Escher's engravings with images from the Poincare disk model of hyperbolic geometry.

Let us return to the theme of the holographic principle in theoretical physics, which was briefly reflected in Fig. 6.6. The work, which is titled “Could a hologram from the holographic principle bend spacetime?”, explains the following [Shiva Meucci, 2020]: “*Holographic principle is a deep and interesting correspondence between two very different versions of modern physics theory: Anti-de Sitter Space (AdS) and Conformal Field Theory (CFT). The reason it’s called holographic principle is the way the two of them fit together is just like a hologram projected off the inside of a sphere. So, the hologram projected inside a circle (an anti-de Sitter space) ... ends up being a crazy fractal looking thing (the author illustrates this phrase by Escher's engraving shown in Fig. 6.11, middle). But that’s just one slice and when we start adding more dimensions we can allow it to evolve over time*». The last phrase about the evolution over time is illustrated by Fig. 6.12, left, wherein the course of considered evolution the Escher's engraving, which symbolically represents the hologram, moves upward along the cylinder, which represents Anti-de Sitter space and has a conformal boundary. This approach of the holographic principle is related to the Poincare disk model of hyperbolic geometry; for this reason, Escher's engraving is used.

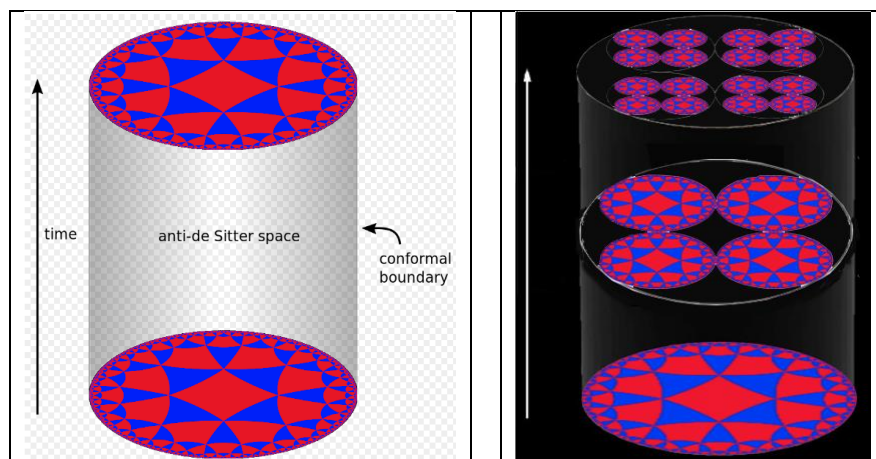


Fig. 6.12. Conditional illustrations of holographic principle models of evolution over time in theoretical physics (at left) and in genetically defined ontogenesis (see explanations in the text). Both illustrations use Escher's engravings since both of them are related to the Poincare disk model of hyperbolic geometry. The straight arrow shows the direction of evolution in time. The image at left is reproduced from <https://commons.wikimedia.org/wiki/File:AdS3.svg> in accordance with the [Creative Commons Attribution-Share Alike 3.0 Unported](#) allowing such reproduction). The image at right is created by the author.

Ontogenesis of a living organism in time is an evolutionary process of its successive complication with a corresponding increase in the number of characteristic parameters (for example, a multicellular organism successive develops from one cell). At the same time, at each stage of such a parametric complication, the organism remains the same due to some algorithmic connection of the parameter systems at different stages of ontogenesis. We put forward a hypothesis that the above-described system of algorithmically and stochastically interconnected n-texts, which exists in any genomic DNA-sequence in a connection with corresponding n-plets alphabets, is related to this ontogenetic complication of organisms.

Fig. 6.12, at right, conditionally illustrates this hypothesis about ontogenesis: a sequence of stages of

an ontogenetic complication of a living body is shown in a form of a sequence of 2^n -dimensional multi-block matrices whose quantity of blocks in each is quickly growing when enlarging n (these are genetic "matrix crystals" from Figs. 6.3, 6.5 about the bit-reversal holography). This hypothesis serves as one of the possible explanations for why each genomic DNA sequence possesses a system of interrelated n -texts written in different alphabets. In this illustration, we use slices of a cylinder by analogy with Fig. 6.12, at left, which illustrates an application of the holographic principles in the mentioned evolution doctrine in theoretical physics.

This article gives some pieces of evidence that the stochastic organization of the holistic genetic system (which has the binary-oppositional molecular indicators of nucleotides jointly with its other above-described molecular features and the universal probability rules in genomes) is connected with the Poincaré disk model of Lobachevsky hyperbolic geometry.

Let us remind some additional information about split-quaternions, Poincaré disk model, hyperbolic motions, and also about known connections of inherited physiological phenomena with hyperbolic geometry. The Poincaré disk model, which is also called the conformal disk model, is related to the hyperboloid model of hyperbolic geometry [Reid, Szendroi, 2005; Reynolds, 1993; https://en.wikipedia.org/wiki/Hyperbolic_motion#Disk_model_motions; https://en.wikipedia.org/wiki/Poincar%C3%A9_disk_model]. Inversive geometry and Möbius transformations are used for describing hyperbolic motions there. The hyperboloid model is also known as the Minkowski model (in a general case it is a model of n -dimensional hyperbolic geometry using a two-sheeted hyperboloid in $(n+1)$ -dimensional Minkowski space).

In connection with Möbius transformations and conformal geometry in our algebra-genetic study, one can recall the phenomenon of conformal-geometric biosymmetries in genetically inherited morphological configurations [Petoukhov, 1989]. Let us also remind that by the pioneering work [Luneburg, 1950], the space of binocular visual perception is described by hyperbolic geometry. These findings were followed by many papers in various countries, where the idea of a non-Euclidean space of visual perception was extended and refined. The Luneburg approach was thoroughly tested by G. Kienle [Kienle, 1964]. In the main series of his experiments, where about 200 observers were involved, Kienle obtained about 1300 visual patterns of various kinds. The experiments confirmed not only that the space of visual perception is described by hyperbolic geometry but also that the Poincaré disk (or conformal) model was an adequate model of that geometry. He concluded his paper by writing: "*Poincaré's model of hyperbolic space, applied for the first time for a mapping of the visual space, shows a reasonably good agreement with experimental results*" [Kienle, 1964, p. 399].

An interesting study about «Non-Euclidean geometries for grid cells» in mammalian brains should be also reminded here [Urdapilleta et al., 2015; Sissa Medialab, 2015]. According to this study, published in *Interface*, the journal of the Royal Society, «*grid cells, space-mapping neurons of the entorhinal cortex of rodents, could also work for hyperbolic surfaces*». This study is coordinated by neuroscientist A. Treves, who notes: "*It took human culture millennia to arrive at a mathematical formulation of non-Euclidean spaces, but it's very likely that our brains could get there long before. In fact, it's likely that the brain of rodents gets there very naturally every day*". The speech is about grid cells, neurons of the entorhinal cortex of rodents that fire in a characteristic way when the animal moves in an arena. The discovery of grid cells by Edvard and May-Britt Moser has been awarded the Nobel Prize in 2014 (for the discovery of the system of cells in the brain, which allows you to navigate in space).

The article [Smolyaninov, 2000] presents the results of 20 years of the author's research on the locomotion of a wide variety of animals and humans. According to these results, spatio-temporal organization of locomotion control is related – in a special manner – with hyperbolic rotations and with Minkowsky geometry. Based on this analysis, Smolyaninov put forward his "Locomotor theory of relativity" and wrote about a relativistic brain and relativistic biomechanics.

The works [Bodnar, 1992, 1994] analyzed growth transformations of geometric lattices in famous morphogenetic phenomena of phyllotaxis, which exist in plant and animal bodies at various levels and branches of biological evolution. On the basis of this analysis, Bodnar declared that living matter is structurally related to Minkowski geometry.

7. Rademacher functions and universal rules of probabilities in n-texts of genomic DNA.

We study the rules of probabilities and the binary-oppositional structure of the genetic system associated with binary numbers and dyadic shifts (see about genetic systems and dyadic shifts in dyadic groups of binary numbers in [Petoukhov, 2016; Hu, Petoukhov, Petukhova, 2017]). But the orthogonal systems of Rademacher functions known in the theory of digital informatics and communication are closely connected with these moments as well [Alexits, 1961; Astashkin, 2020; Kac, 1959; Kaczmarz, Steinhaus, 1951; Wolfram, 2002].

The close connection of the Rademacher functions with the theory of probability is demonstrated by the known fact that every statement about the Rademacher functions can be interpreted from the point of view of the theory of probability [Alexits, 1961, §7]. The interval $[0, 1]$ is a key interval for both of them: it contains values of genomic probabilities and it is the interval for determining the Rademacher functions as well. One should also note the following analogy: each of the DNA-alphabets of n-plets contains 4^n members of identical length n, and each of Rademacher functions is determined at the interval $[0, 1]$, which is divided on 2^n fragments of equal length. These analogies define a necessity to study interconnections between Rademacher functions and genomic rules of probabilities jointly with special structures of DNA-alphabets of n-plets. This section describes the initial author's results of such a study.

The Rademacher function $f_n(x)$ is defined on the closed interval $[0,1]$ by the Equation (7.1):

$$f_n(x) = \text{Sgn}[\sin(2^n x)], n = 0,1,2,3,\dots \quad (7.1)$$

where $f_0(x) = 1$; Sgn = the signum function equation: $\text{Sgn}(y) = +1$, if $y \geq 0$, and -1 , if $y < 0$.

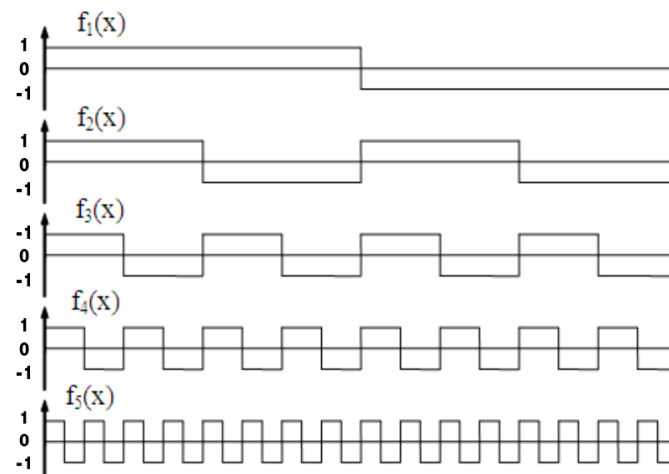


Fig. 7.1. First five Rademacher functions.

Rademacher functions are connected with Walsh functions and Hadamard matrices, which are intensively used in the theory of digital signals including many methods of noise-immunity coding of digital information. Walsh functions, which, in particular, represent rows or columns of Hadamard matrices, can be defined via multiplications of Rademacher functions on each other. A system of Rademacher function is orthogonal. For example, one can consider two Rademacher functions $f_2(x)$ and $f_4(x)$, which are defined on the identical interval $[0, 1]$ (Fig.7.1), as vectors F_2 and F_4 in a 16-dimensional vector space: $F_2 = [1, 1, 1, 1, -1, -1, -1, -1, 1, 1, 1, 1, -1, -1, -1, -1]$ and $F_4 = [1, -1, 1, -1, 1, -1, 1, -1, 1, -1, 1, -1, 1, -1, 1, -1]$. These two Rademacher vectors are mutually orthogonal: their dot product is zero.

One should remind that, in the theory of digital signals, signals are represented by a sequence of numerical values of their amplitude at points of reference since this theory is based on the representation of discrete signals in the form of vectors of multidimensional spaces: the value of the signal at each cycle is interpreted as the value of one of the coordinates of a vector in the multidimensional space of signals. The theory of discrete signals turns out to be in many respects the science of the geometries of multidimensional spaces. The dimension of such a space is equal to the number of points of reference for the signal. For these multidimensional vector spaces, metric concepts and, in general, everything necessary for tasks of ensuring reliability, speed, and efficiency in the transmission of signal information are introduced. For example, the

concepts of energy and power of a discrete signal, important for informatics, turn out to be nothing more than the square of the length of the multidimensional signal vector and the square of the length of the signal vector divided by the dimension of the signal multidimensional space. Various transmitted and received signals and their ensembles are compared in digital technologies as geometric objects of such metric multidimensional spaces. Methods and algorithms for recognizing signals and images, identifying and correcting information errors, artificial intelligence and teaching robots, etc. are built on this.

Fig. 7.1 shows that Rademacher functions have periodic patterns of a regular meander type: in each of them, a length of intervals with its value +1 is equal to a length of intervals with its value -1. One of the mysterious phenomena of the organization of the genetic coding system lies in the many connections of its ensemble structures with regular meander patterns that coincide with meander patterns of Rademacher functions. Some examples of such meander patterns are given by all the mosaic rows of genetic matrices in Figs. 6.1-6.3, 6.9, in which the length of a row fragment of one color is equal to the length of a fragment of the next fragment of the row. The article [Petoukhov, 2021b] gives many other examples of meander-like patterns in all the rows of genetic mosaic matrices, which illustrate the universal tetra-grouping rules of probabilities of n -plets in n -texts of DNA of eukaryotic and prokaryotic genomes. Some of the mentioned patterns are reproduced below in Fig. 7.2.

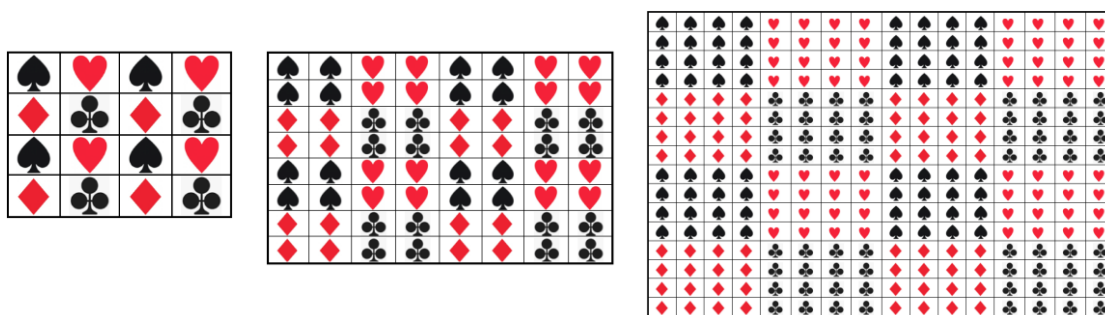


Fig. 7.2. The arrangements of n -plets, which form tetra-groupings of probabilities of n -plets in n -texts of genomic DNA, in the matrices of the tensor family $[C, A, T, G]^{(n)}$ under $n = 2, 3, 4$ (from [Petoukhov, 2021b, Fig. 7.10] where a detailed explanation exists). These images were created by the author.

This genetic phenomenon of existing regular meander patterns of Rademacher functions in many genetic mosaic ensembles should be specially studied in the future. In his previous publications, the author connected relations of the genetic meander patterns of the Rademacher type with the orthogonal system of Walsh functions and Hadamard matrices but, perhaps, additional reasons exist for such phenomena [Petoukhov, 2008; Petoukhov, He, 2010].

8. Genetic stochastic resonance in algebraic biology

One of the fundamental biological questions is the question of how the information, which is recorded at the level of DNA molecules, is essentially amplified to dictate the features of physiological macrostructures. In this section, the author puts forward and arguments a concept about an important role of stochastic resonances in this amplification (though it is not excluded other amplification mechanisms in the field of genetic informatics). This concept arose from the author's mind as a result of combining him the following four heterogeneous facts of genetics: 1) discovered by him the universal rules of probabilities in the DNA of the eukaryotic and prokaryotic genomes, existing against the background of internal electromagnetic, vibrational and acoustic noises of organisms; 2) the well-known fact that an organism is a set of genetically encoded cyclic processes that respond to external periodic influences, for example, a change in solar activity in the daily cycle "day-night"; 3) the non-linear system of structured alphabets of n -plets of DNA is built on binary-oppositional principles, conjugating with binary numbers and Rademacher functions, closely related to the theory of probability; 4) the information, recorded at the level of DNA molecules, is somehow significantly amplified to dictate the features of the macrostructures.

But the physical and informational phenomenon of stochastic resonance described below is also based on the combined action of noise and cyclic processes in nonlinear systems and provides an amplification of

weak signals. Let us explain this in more detail.

The concept of resonance is one of the long-known fundamental concepts of science. But relatively recently - in 1981 - a new important concept of "stochastic resonance" entered science [Benzi, Sutera, Vulpiani, 1981; Benzi, Sutera, 2004; Benzi, 2010; Nicolis, 1982]. It reflects a physical phenomenon, the existence of which was confirmed in subsequent years by many authors. Over the past time, this concept has proven its usefulness in various fields of knowledge and has taken a prominent place in modern science. More than 13,000 publications have been devoted to the theory and applications of stochastic resonance, including a series of articles in the journal Nature. In this section, the author notes only some of them to demonstrate the relationship of the phenomenon of stochastic resonance with genetically inherited physiological systems, as well as the relationship of this phenomenon with the structures and principles of the work of genetic informatics. Below we initially describe some general data about stochastic resonance and then turn to questions of stochastic resonance in biological objects.

- 8.1. Introduction data about stochastic resonance.

Stochastic resonance (SR) is usually described as the phenomenon of amplification of a periodic signal in nonlinear systems under the influence of noise of a certain power [https://en.wikipedia.org/wiki/Stochastic_resonance]. It is accompanied by the transfer of some of the noise energy into signal energy, which increases the energy of the weak signal without suppressing noise. The work [Benzi, 2010] contains some illustrations of stochastic resonance with a partial injection of noise energy into the weak signal. The author who discovered this phenomenon explains: *«In some sense, stochastic resonance is a counter-intuitive phenomenon because without noise the system shows a small amplitude modulation around one of the two stable steady states ± 1 , while adding the noise we obtain a large amplitude effect with the same period»* [Benzi, 2010, p.434]. And further: *“Note that stochastic resonance is a mechanism in the full meaning of the word because it allows to get large effect from a small amplitude perturbation. There have been and still are many applications of stochastic resonance to problems dealing with the amplification of signal to noise ratio, a quite traditional engineering problem... Stochastic resonance is a counter-intuitive phenomenon: it is not trivial that adding noise to a system we can enhance the deterministic periodic behavior. Stochastic resonance is a robust mechanism, observed in many physical and biological systems. The notion of stochastic resonance is now cross disciplinary and new applications are found every year”* [Benzi, 2020, p. 440].

The occurrence of stochastic resonance can be controlled by adjusting the appropriate parameters, for example, the intensity of the excitation noise, the structure and parameters of nonlinear systems [Lin Cui, et al., 2021]. A popular presentation of the features of stochastic resonance and its applications is given on the site [http://www.scholarpedia.org/article/Stochastic_resonance]. Let's reproduce several fragments from it. Stochastic resonance is a mechanism by which a system embedded in a noisy environment acquires an enhanced sensitivity towards small external time-dependent forcings when the noise intensity reaches some finite level. As such it highlights the possibility that noise, a universal phenomenon and yet one considered traditionally to constitute a nuisance, may actually play a constructive role in large classes of both natural and artificially designed systems. ... Spatially extended systems of coupled bistable elements are widely spread in nature and technology, from neurophysiology to computer science. Under the presence of noise and an external periodic forcing the stochastic resonance that would be observed in the limit of totally independent elements is further enhanced by the spatial coupling, the enhancement being at a maximum for a certain well-defined finite coupling strength. ... The Quantum Stochastic Resonance phenomenon requires some amount of asymmetry. For symmetric systems, it can occur nevertheless but then requires sufficiently strong quantum friction. ... Stochastic resonance is a generic phenomenon. It has to do with the fact that adding noise to certain types of nonlinear systems possessing several simultaneously stable states may improve their ability to process information. As such, it is at the origin of intense interdisciplinary research at the crossroads of nonlinear dynamics, statistical physics, information and communication theories, data analysis, life and medical sciences. It opens tantalizing perspectives, from the development of new families of detectors to brain research. From the fundamental point of view, it is still a largely open field of research. Its microscopic foundations have been hardly addressed, its quantum counterpart needs to be further elucidated,

and its relevance in global bifurcations and in complex transition phenomena in spatially extended systems remains to be explored.

By now, various authors have developed models and theories of stochastic resonance for cases of signals of complex spectral composition, aperiodic stochastic resonance, stochastic resonance as a fundamental threshold effect, stochastic resonance in chaotic systems, the synchronization of stochastic systems by stochastic resonance, stochastic synchronization as noise-induced order, etc.

- 8.2. Stochastic resonance in genetically inherited physiological systems.

As noted in the work [Anishchenko et al., 1999], from a fundamental scientific point of view, applications of the stochastic resonance theory to the study of information processing by biological systems are of the greatest interest. There is reason to believe that in the process of evolution, living organisms have adapted to use the unavoidable internal noise and the noise of the environment for optimal identification of useful information. " This statement is supported by the results of a study of sensory processes in hydrodynamically sensitive mechanoreceptors of crayfish [Douglass et al., 1993; Pei, Wilkens, Moss, 1996] and cricket air-sensing receptors [Levin, Miller, 1996]. It is noted that the process of transferring information from the stimulus signal to neurons occurs in the best way at a certain optimal level of external noise; furthermore, adding external noise to the weak periodic signal can also improve the time-coding accuracy of the signal in the action potential burst sequence.

The same article indicates that an ensemble of stochastic resonators, in contrast to a single bistable element, demonstrates the effect of stochastic synchronization with an arbitrarily weak external periodic signal. In addition, in the ensemble, the frequency dependence of the coherence function disappears with an increase in the number of elements. This conclusion is very important since it removes the question of how living organisms can use the SR effect without "adjusting" the noise level.

SR is also used to explain the physiological phenomena of synesthesia and the mutual influence of various sensory systems on each other [Krauss, et al., 2018]; for example, the phenomenon of a significant improvement in speech perception thresholds during electro-tactile stimulation of the index finger. The authors believe that stochastic resonance plays a key role in auditory processing and takes place in the dorsal cochlear nucleus. There are great prospects for the use of SR in understanding auditory perception and a number of its disorders. Based on their observations and the data of other researchers in the works indicated in the bibliography to the named article, the authors believe that stochastic resonance in one sensory modality, controlled by input from another modality, can be a general principle, namely, the principle of multisensory integration, causing stochastic resonance as a cross-modal enhancement. For example, similar to somatosensory enhancement of auditory perception, visual perception at exposure thresholds can be enhanced by auditory stimulation, and even visual stimuli below the threshold level may be sensed through spatially converging audio-visual inputs. This audiovisual cross-modal improvement in detection thresholds has been demonstrated in a wide variety of different organisms, for example, ferret and chicken.

The existence of SR has been demonstrated not only in systems of the macroscopic level but also at the molecular level [Bezrukov, Vodyanoy, 1997; Moss, 1997]. Some authors discuss the question of the probable role of SR in the phenomenon of hypersensitivity of some organisms to weak signals in noisy environments, as well as the possible role of SR in the problem of the influence of electromagnetic fields on human and animal health. [Wiesenfeld, Moss, 1995].

The following well-known example of a universal and genetically inherited function of all warm-blooded animals can also be attributed to the category of phenomena of stochastic resonance in biology: this is an involuntary muscle tremor on cooling, which creates muscle and neural noise and leads to the release of the hormone irisin. With tremors, almost three times more heat is generated than at rest. As established by the specialists of the US National Institutes of Health, the subcutaneous muscles, which contract with tremors, secrete the hormone irisin, which signals the fat cells that it is time to speed up metabolism and release heat. (https://www.gazeta.ru/health/2014/02/06_a_5884077.shtml). As it is known, there are several factors of contractile thermogenesis: thermoregulatory muscle tone, muscle tremors, and voluntary muscle contractions. The tone is determined by the degree of activity of the muscles that do not perform visible work. It is believed that voluntary contractions, controlled by a conscious effort of will, are less effective at raising body temperature than shivering, which is uncoordinated and multidirectional contractions of muscle fibers

(<https://postnauka.ru/faq/71757>). It turns out that the task of muscle tremors is to create noise! This specialized noise by the stochastic resonance mechanism can promote the excitation of the threshold system of neural signals for the release of the hormone irisin for thermogenesis.

The work [Dubkov, 2014] notes the following:

- in the early 90s in science it was realized that stochastic resonance can play a key role in the functioning of neural networks and in the transfer of information from one group of neurons to another;
- Numerical calculations performed in [Longtin, 1993] on the FitzHugh-Nagumo neuron model confirmed the presence of stochastic resonance in the histogram of interspike intervals;
- The mechanism of noise-induced order was found even in the human thought process [Usher, Feingold, 2000];
- Noise-induced phenomena are found directly in the part of the brain responsible for image processing. It has been found [Mori, Kai, 2002] that the illumination noise directed to the left eye improves the processing of the periodic signal sent to the human right eye.
- Experiments in Boston University [Collins, Imhoff, Grigg, 1996; Priplata, et al., 2002] have convincingly shown that subthreshold tactile noise (that is, weak random vibrations, in themselves imperceptible by the patient) can sharpen the sense of balance when walking. This means that special shoes with chaotically vibrating inlays in the sole can improve coordination of the elderly or people with balance disorders.

Currently, stochastic resonance is actively used in medical clinics and centers in Germany, the United States, and other countries for the treatment of many types of health disorders.

- 8.3. Genetic stochastic resonance.

The creators of quantum mechanics P. Jordan and (later) E. Schrödinger pointed out the key difference between living bodies and inanimate ones: inanimate objects are controlled by the average random motion of their millions of particles and the motion of individual particles is not essential for the whole; on the contrary, in a living organism, the chosen - genetic - molecules have a dictatorial influence on the entire organism due to special amplification (see the history of "quantum biology" [McFadden, Al-Khalili, 2018]).

The question of the mechanisms of this amplification, which allows genetic information from the level of DNA molecules to dictate the features of macroscopic biostructures, is one of the most important fundamental questions in the science of life. The author believes that stochastic resonance (SR) is one of the prominent participants in this amplification. This section presents arguments for this proposition put forward by him, which supplements the known data on the relationship of the genetic coding system also with the theory of classical resonances of oscillatory systems with many degrees of freedom [Petoukhov, 2016].

As described above, there are many facts obtained by various authors about the participation of stochastic resonance mechanisms in the functioning of physiological systems. But all physiological systems are genetically inherited by descendants, thanks to genetic coding, and therefore bear the features of the structures of genetic coding. In light of this, it is natural to believe that the mechanisms of stochastic resonance are represented in the nonlinear genetic coding system, and therefore, taking them into account can clarify some of the features of its structure and functioning, including the aforementioned dictatorial influence of DNA molecular information to macroscopic biostructures.

The phenomena of genetic inheritance of physiological structures form a specific class of natural phenomena, in which the mechanisms of stochastic resonance have their own quantitative and another specificity. As noted above, living organisms are fundamentally different from inanimate ones due to the dictatorial influence of genetic DNA and RNA molecules. For this reason, the author introduces the concept of "genetic stochastic resonance" (GSR) defined as such special case of the general concept of stochastic resonance (SR), which unites many specific manifestations of stochastic resonance mechanisms in genetic phenomena, allowing the study of their interrelationships within the framework of the concept of the integrity of the organism and dictatorial the influence of DNA. The concept of GSR pays special attention to the theory and applications of SR for systems of genetic helical and spiral biostructures with their signal and noise electromagnetic waves of circular polarization, which are generated and received by them for mutual communication and coordination.

Stochastic resonance in nonlinear systems connects noise, as a phenomenon of a probabilistic type, with deterministic processes (primarily periodic), the amplitudes of which are amplified when they are superimposed on noise (under certain combinations of temporal parameters of noise and cyclic influences).

But in the genetic system, which is nonlinear, both types of phenomena of the organization of genetic information coexist - probabilistic and deterministic:

- In the genomes of higher and lower organisms, universal algebraic rules of probabilities have been identified, which remain unchanged, according to the data available today, for millions of years of biological evolution [Petoukhov, 2021a,b]. Moreover, these universal rules for the probabilities of genomic tetra-groupings testify to the fact that specially organized electromagnetic and other noises, coupled with the piezoelectric properties of many biological tissues, operate in genetics. In addition, the system of structured genetic alphabets is associated with binary numbers and Rademacher functions, which are also connected with the theory of probability;
- Many genetic processes are stochastic. In particular, gene expression is an intrinsically stochastic process, which is conditioned by the probabilistic occurrence of molecular interactions and reactions and accompanied by stochastic physical and chemical signals;
- Biosynthesis of proteins from amino acids in ribosomes based on data from DNA and RNA is cyclical, like many other physiological processes; the organism as a whole is a huge chorus of mutually coordinated cyclical processes, and all our diseases, according to chrono-medicine, are the result of violations of their coordination.

To the rich topic of studying the relationship of genetic stochastic resonance with cyclic processes in the body, it can be added that the proteins of the body, built following DNA information, are participants in the life-death cycles. The point is that the proteins of the body are constantly broken down into amino acids and recreated again. Only a third of the synthesis of proteins in the body is accounted for by amino acids supplied with food. The half-life (the time during which half of the protein molecules are renewed) is usually about 80 days for the proteins of the human body, ten days for the proteins of the liver and blood plasma, three to four days for the intestinal mucosa, and six to nine minutes for the insulin hormone (such concrete periods of inherited cyclic processes should be taken into attention in the development of the theory of genetic stochastic resonance and its possible biotechnological applications). This constant digestion of one's own and "foreign" proteins ensures organism continuous renewal. Accordingly, the architectural structures made of proteins in the body, for example, the cytoskeleton, are constantly being rebuilt, which is fundamentally different from ordinary building structures created by man from static building beams [Fulton, 1984]. Taking into account such phenomena, the well-known physiologist A.G. Gurvich argued: "*The main problem in biology is maintaining shape while constantly renewing the substrate*" [Gurvich, 1977].

The cyclic life of proteins in the body is usually completely hushed up in the genetic coding literature, which focuses only on the assembly of proteins from a genetically encoded sequence of amino acids without mentioning the genetic mechanisms of cyclic disassembly of proteins. However, it seems that genetically encoded not only the assembly of proteins in the first half of the cycle "assembly-disassembly" of protein but also the entire cycle, including its second half - protein disassembly. One can believe that the theory of genetic coding in the future will present the phenomenology of the genetic code precisely in connection with the coding of this complete cycle, and chronocyclic aspects of protein lives will be also included in the scope of this theory.

Let us recall that the process of transformation of a sequence of DNA triplets into amino acid chains of proteins is not of a one-step nature, but has many intermediate stages, which are ensured by the coordinated work of a large number of auxiliary biochemical agents (primarily enzymes and nucleic acids). These agents are undoubtedly endowed with some kind of interrelated rhythms of activity within the framework, first of all, of a daily cycle with a total period of 24 hours. The high coherence of the cyclic functioning of this multitude of intermediate agents in the biochemical "cauldron" of genetic coding is only just beginning to be studied by modern science and has many mysteries.

This consistency of the rhythms of many separate processes of storage and transmission of hereditary information, which ensures the cyclic assembly and disassembly of proteins, can determine the number of structural features of the genetic code in their conjugation, in particular, with a 24-hour duration of the day. Indeed, it is to the daily cycles of solar activity - sunlight during the day and its absence at night - that the photosynthetic mechanisms of autotrophic organisms should be obeyed; these organisms use CO₂ as the only or main source of carbon to build their body. These cyclic photosynthetic mechanisms and processes in autotrophic organisms are basic for living nature and they are coordinated with the daily solar day-night cycles. They can serve as the "bridge" through which solar daily and seasonal cycles influenced, in particular, genetic structures and cyclic processes of reading and realization of genetic information.

Let us recall that *“the role of photosynthetic autotrophic mechanisms in nature is decisive because they form the bulk of organic matter in the biosphere ... The activity of autotrophic mechanisms determines both the existence of all other organisms and the course of biogeochemical cycles in the circulation of substances in nature”* [Gilyarov, 1989, p.9]. So, autotrophic mechanisms are of decisive importance in comparison with heterotrophic organisms, which use exogenous organic substances as a carbon source and which, therefore, can be adapted, in principle, to other - not solar - cycles of activity. This importance of autotrophic organisms was taken into account by the author during the analysis of the degeneracy of the known dialects of the genetic code in [Petoukhov, 2001, 2005].

But where and how can you find traces or imprints of the 24-day "day-night" cycle on the structures of the genetic code, which can be realized in them through the mechanisms of stochastic resonance? Is it possible, for example, to interpret individual groups of triplets encoding the same amino acid or a group of amino acids as separate "organs" that have increased functional activity within 24 hours of a day at certain time intervals by analogy with the cycles of "activity-rest" or "wakefulness-sleep" in many physiological systems of the body? In this case, of course, the cyclic activity of these "organs" is associated with the accompanying cyclic activity of the entire group of biochemical agents, which ensures the reading and implementation of these triplets during the creation of proteins. Recall that *“a necessary condition for protein synthesis, which ultimately comes down to the polymerization of amino acids, is the presence in the system of not free, but so-called activated amino acids, which have their internal energy reserves. Free amino acids are activated by specific enzymes”* [Berezov, Korovkin, 1990, c. 409]).

Attempts to find along this path traces of chrono-cycles associated with the cycle of 24 hours of the day led the author to a comparative analysis of the degeneracy numbers for amino acids in all variants of the genetic code known at the time of the study. As a result, several nontrivial numerical rules for the evolution of the genetic code were identified [Petoukhov, 2001, 2005]. The author believes that the daily cycles of solar activity are participants in genetic stochastic resonances, which are important for structuring the genetic coding system.

Many such facts speak in favor of the connection between epigenetics and stochastic resonance, which naturally connects the internal noise oscillations of the organism with external periodic and noise influences and is able to cause a certain restructuring of cyclic processes inside the organism. In this case, the development of the body turns out to be dependent on external influences such as daily fluctuations in temperature, lighting, cyclic locomotion, phases of sleep and wakefulness, etc. Many periodic influences on the whole organism, generated by its muscular and other activity, for example, locomotor movements also change their characteristics with age. For different types of organisms, for example, animals and plants, external cyclic and noise effects can be selected, which, through interaction with their specific internal genetic noises and cycles, optimize their functions necessary for agriculture, medicine, and technology. In our opinion, the long-known vibration medicine, presented in many publications, for example, in the book *“Vibration Medicine”* [Gerber, 1996], also acts through the mechanisms of stochastic resonance.

The topic of epigenetics is also associated with the problems of ontogenesis and aging. Let's talk about this in more detail. Different types of cells in our body contain a set of DNA of the same nucleotide composition. However, the types of cells that develop during ontogenesis in the liver, skin, hair, and many other parts are very different. The explanation for this is given by the well-known idea that not all DNA double helix is a homogeneous supercoiled structure, but it contains fragments of a relatively untwisted (straightened) form protruding outward from the general supercoiled structure in a form of loops (see, for example, illustrations in <https://www.youtube.com/watch?v=BUJHgiThKaU>).

The genes contained in such loops are available for expression (that is, the realization of their information for the synthesis of the corresponding proteins) under the influence of molecular epigenetic agents that surround DNA in the cell. Different types of cells differ in the set of these DNA loops and, accordingly, in the expression of different genes, which entails a different ensemble of realized proteins in each species. In the same cell, the configuration settings of these DNA loops, which dictate the current synthesis of kinds of proteins, are changed during ontogenesis. Some authors believe that age-related changes in the sets of such DNA loops in cells, which alter the synthesis of kinds of proteins, cause the aging of the organism. Research is currently underway in various laboratories to rejuvenate the body by returning sets of these DNA loops to sets of DNA loops of a younger age (see, for example, <https://youtu.be/TSK374Kn11k>). This understanding of the configurational differences in DNA in different types of cells of the body (with the identity of the

nucleotide composition of DNA) covers also the issue of the phenomenon of stem cells that are capable of transforming into different types of cells in the body.

It is natural to think that genetic stochastic resonance, due to its influence on these configuration sets of cell DNA loops, can act as one of the epigenetic mechanisms. The author believes that, taking into account the genetic characteristics of specific biological objects and selecting the necessary noise and signal modes of genetic stochastic resonance, this resonance can be used to control the transformation of stem cells into other types of cells for biotechnological, medical, and other purposes. Moreover, one can think that genetic stochastic resonance is involved in the biological self-organization of the appearance of such DNA loops in the cell due to noise and cyclic influences existing in the cell itself and in the surrounding biological media. With a broader view, it can be assumed that the self-organization of biological bodies uses a whole system of genetic stochastic resonances interacting with each other.

There are many types of noise: sound, light, vibration, electromagnetic, ... Each of them, when interacting with external periodic influences or internal periodic processes - under certain conditions of coordination of their quantitative characteristics - causes in nonlinear systems an increase in periodic phenomena of the corresponding physical modality due to stochastic resonance.

According to the author, many well-known physiological phenomena and traditions of folk and European medicine, culture, and religions, associated with cyclical processes and noises, need to be considered and comprehended in connection with genetic stochastic resonance, including, for example, the following:

- the mother rocks the child to calm him down - it is a method used all over the world to calm the child;
- the phenomenon of motion sickness (motion sickness), accompanied by dizziness, nausea, and a desire to avoid movement (to be motionless);
- the tradition of dancing, which exists among all peoples and at all times based on rhythmic movements to rhythmic music;
- the tradition of shamans to move rhythmically to the rhythmic beat of a tambourine to enter special states to communicate with spirits;
- the tradition of Buddhists to beat rhythmically with a mallet, tambourines, and ring bells;
- mutual consistency of biorhythms and synchronization of processes in different subsystems of the body, including cardiac and respiratory;
- therapeutic use of the impact of electromagnetic and other wave fields on living organisms.

The next section examines the human affinity for music, which is also desirable to comprehend taking into account the mechanisms of genetic stochastic resonance.

- 8.4. Genetic stochastic resonance and inherited human affinity with music

The specificity of genetically inherited cyclic molecular processes in the body gave rise to the term "biochemical aesthetics" [Shnoll, 1979, p.75]: *"From possible consequences of interaction of macromolecules of enzymes, which are carrying out conformational (cyclic) fluctuations, we shall consider pulsations of pressure - sound waves. The range of numbers of turns of the majority of enzymes corresponds to acoustic sound frequencies. We shall consider ... a fantastic picture of "musical interactions" among biochemical systems, cells, bodies, and a possible physiological role of these interactions. It leads to pleasant thoughts about nature of hearing, about an origin of musical perception and about many other things, which belong to area of biochemical aesthetics already"*.

The term "biochemical aesthetics", which was introduced by professor of biophysics E.Shnoll, touches upon the historical phenomenon of human affinity with music, which can be considered from the standpoint of genetic stochastic resonance. Here the following questions arise:

- Is there a historical basis for thinking about musical harmony in a living organism?
- Does the molecular genetic coding system have an interrelation with the harmony of musical tunings (or scales) and, if so, with which of the many known or possible tunings?

There is no specialized music center in the human brain, the feeling of love for music is dispersed throughout the body (like as DNA molecules) and has accompanied people of different nationalities and tribes since ancient times. More than 30 thousand years ago, long before the advent of arithmetic, our ancestors already played stone flutes and bone harps.

In Europe, since the time of Pythagoras, the concept of musical harmony has been associated with the Pythagorean 7-step musical system do-re-mi-fa-sol-la-si. The sound frequencies of its notes, when spaced into

different octaves, are mathematically mutually related strictly based on the ratio 3:2, called the fifth (or the quint) in musicology (Fig. 8.1). In general, any tuning is called Pythagorean, which can be constructed on the basis of only the ratio 3:2 and the octave ratio 2:1. Recall that in musical scales, the ratio of adjacent sound frequencies of the scale is important, and the absolute value of individual sound frequencies is not important.

Фа	До	Соль	Ре	Ля	Ми	Си
87	130	196	293	440	660	990
$(3/2)^{-3}$	$(3/2)^{-2}$	$(3/2)^{-1}$	$(3/2)^{-0}$	$(3/2)^1$	$(3/2)^2$	$(3/2)^3$

Fig. 8.1. The quint (or the fifth) sequence of the 7 notes of the Pythagorean musical scale. The upper row shows the notes. The second row shows their frequencies. The third row shows the ratios between the frequencies of these notes to the frequency 293 Hz of the note re (D¹). The designation of notes is given on Helmholtz system. Values of frequencies are approximated to integers.

Other examples of Pythagorean musical tunings are pentatonic, tetratonic, and tritonic, the sets of sound frequencies in which are mutually related by the noted ratio 3: 2. It is a well-known historical fact that these musical scales were used by various civilizations around the world long before Pythagoras without knowledge of any mathematical laws. For example, the mentioned Pythagorean scales are the basis of the traditional music of China, Vietnam, Mongolia, Turkey, the Southern Andes, Polynesia, Melanesia, Indians, the Inca empire and many others (for more details, see [Petoukhov, 2019b]). This fact speaks of the innate universal genetic affinity of people with musical scales based on the ratio 3:2. But is there anything in the genetic system that can explain this universal implementation of the Pythagorean scales, based on the ratio 3:2, in the musical culture of different civilizations and eras? Yes, there is. Let us explain this.

It is known that a pair of these numbers 3 and 2 is embodied by nature in the structure of information sequences of DNA molecules of all organisms. These sequences consist of four types of nucleotides (“letters”): adenine A, cytosine C, guanine G, and thymine T. In the DNA double helix, nucleotides AT and C-G form complementary pairs with 2 and 3 hydrogen bonds between them, respectively. In terms of the sequence of these two and three hydrogen bonds, each DNA molecule is a long chain of numbers 2 and 3 (Fig. 8.2).



Fig. 8.2. The quint sequence of numbers 2 and 3 of hydrogen bonds in the DNA double helix.

Genetic coding of protein amino acid sequences is carried out by 64 triplets, in the form of all possible combinations of these four letters by three (ATC, TTA, ...). When nucleotides are represented by their numbers of hydrogen bonds $A = T = 2$, $C = G = 3$, each triplet receives a numerical representation in the form of the product of the numbers of hydrogen bonds of its constituent nucleotides. For example, the triplet ACT is represented by the number $2 \cdot 3 \cdot 2 = 12$. In such representation, each of the 64 triplets is represented by one of the “hydrogen” numbers $2^3 = 8$, $2^2 \cdot 3 = 12$, $2 \cdot 3^2 = 18$, $3^3 = 27$, pairwise ratios between which are equal to the quint value $3/2$ in various integer degrees (by analogy with the musical structure of tetratonics), for example, $27/8 = (3/2)^3$, $18/8 = (3/2)^2$, etc.

When analogically considering 6-plets, the DNA sequence of hydrogen bonds appears, respectively, as a quint sequence of 7 types of hydrogen bond numbers: $2^6 = 64$, $2^5 \cdot 3 = 96$, $2^4 \cdot 3^2 = 144$, $2^3 \cdot 3^3 = 216$, $2^2 \cdot 3^4 = 324$, $2 \cdot 3^5 = 486$, $3^6 = 729$. Pairwise ratios in this series of numbers are equal to the quint value $3/2$ in various integer powers in exact analogy with the Pythagorean 7-step system in Fig. 8.1. Accordingly, each DNA molecule - like a chain of hydrogen bonds - is characterized by its sequence of the quint value $3/2$ in

different integer degrees, which can be sounded in the notes of this Pythagorean quint system in Fig. 8.1. Considering similarly the DNA sequences of 4-plets, 5-plets, 7-plets, and so on, we each time obtain sequences of numbers, which relate to each other in line with the quint value $3/2$ in various integer degrees, like sound frequencies in the corresponding Pythagorean micro-chromatic musical scales.

But the quint ratios in DNA are realized by nature not only for the sequences of hydrogen bonds of complementary nucleotides but also for some other molecular parameters, for example, the sums of atoms in the rings of purines and pyrimidines (numbers 9 and 6, giving the ratio $3/2$), the sums of protons in the rings complementary nitrogenous bases (numbers 60 and 40, giving the ratio $3/2$), etc. In other words, nature created DNA as an interweaving of various sequences of quint ratios, that is, as quint “polyphony” [Petoukhov, 2008; Petoukhov, He, 2010]. Accordingly, the harmony of the parametric organization of DNA turns out to be akin to the musical harmony of the Pythagorean quint tunings, on which the “spontaneous” folk music of different civilizations and eras is based.

From the standpoint of the idea of genetic stochastic resonance, this need of people of different eras to compose and perform music based on quint scales can be considered as the need for a person to create external sound influences of a quint character for optimizing of genetically inherited physiological processes in his body by instinctive use of the mechanisms of genetic stochastic resonance.. On the other hand, the mechanisms of stochastic resonance can be considered in connection with the internal noises of the body as amplifiers of signal information from the named quint sequences of DNA signal elements for the construction - on the basis of this amplified information - of a coordinated set of cyclic processes at the physiological macrolevel. It is possible that the harmonic progression $1, 1/2, 1/3, \dots, 1/n$, associated with the harmonics of music and phenomenologically represented in the universal rules for the probabilities of n-plets in n-texts of genomic DNA [Petoukhov, 2019b, 2020a-c, 2021], can also be associated with the mechanisms of genetic stochastic resonance.

We also note that the Pythagorean musical scales, based on the quint ratio $3/2$, are mathematically closely related to another type of musical scales, called Fibonacci-stages scales or pentagram scales [Petoukhov, 2008; Petoukhov, He, 2010]. These two types of musical scales appear to be of particular interest for future research and biotechnological applications of genetic stochastic resonance. In these tasks, it is useful to use the well-known works on the generation of order by noise in the case of stochastic synchronization with the participation of stochastic resonance.

Based on genetic stochastic resonance, we can influence the state of living organisms (for example, animals and plants in agricultural tasks) in two ways or a combination of them: 1) creating the necessary additional noises from the outside; 2) creating external periodic influences of the necessary parameters and physical types (sound, light, electromagnetic, etc.), which are quantitatively consistent with internal physiological noises.

9. Some concluding remarks.

The discovered universal rules of probabilities and symmetries in the conjugation of the percentage compositions of n-plets in n-texts of DNA of eukaryotic and prokaryotic genomes indicate that the foundations of genetic coding are based on special interconnected probability systems and ensembles of binary oppositions.

An important role in the systemic organization of genetic informatics is played by the tensor product, which appears in one of the postulates of quantum mechanics: the state space of a composite system is the tensor product of the state spaces of its components. Taking this into account brings genetic informatics closer to mathematical formalisms of quantum informatics and of quantum mechanics and leads to the mutual enrichment of these sciences.

The development of knowledge about algebraic-holographic principles in the ensemble structures of a molecular genetic system makes it possible to deeper comprehend the nonlocally informational (holographic-like) properties of inherited physiological systems, including the brain.

The applications of the concept of genetic stochastic resonance described in the article to the analysis of the characteristics of genetic phenomena and inherited physiological systems indicate the existence of a vast field of research of fundamental and applied importance. The results of new studies currently being carried out at the Department of Vibration Biomechanics and the author's laboratory of biomechanical systems at the Mechanical Engineering Research Institute of the Russian Academy of Sciences will be published later.

The author also carries out these studies with collaborators at the Moscow Tchaikovsky State Conservatory on the basis of the "Center for Interdisciplinary Research of Musical Creativity".

Appendix I. On the tensor product of matrices.

The tensor (or Kronecker) product of matrices, denoted by \otimes , is widely used in mathematics, theoretical physics, informatics, control theory, etc. In a general case, if K_1 is an $(m \times n)$ -matrix and K_2 is a $(p \times q)$ -matrix, then the tensor product $K_1 \otimes K_2$ is the $(mp \times nq)$ -block matrix:

$$K_1 \otimes K_2 = \begin{vmatrix} \underline{a_{11}K_2} & \dots & \underline{a_{1n}K_2} \\ \vdots & \ddots & \vdots \\ \underline{a_{m1}K_2} & \dots & \underline{a_{mn}K_2} \end{vmatrix}$$

Fig. A1. The definition of the tensor product of two matrices K_1 and K_2 .

The tensor product is the crucial operation to understanding the quantum mechanics of multiparticle systems and is one of the basic instruments in quantum informatics. The following quotation speaks about the tensor product: «*This construction is crucial to understanding the quantum mechanics of multiparticle systems*» [Nielsen, Chuang, 2010, p. 71] since in line with the postulate of quantum mechanics: the state space of a composite system is the tensor product of the state spaces of its components.

This operation has the following important property for square matrices: if a $(n \times n)$ -matrix K_1 has eigenvalues s_j ($j=1, \dots, n$) and another $(m \times m)$ -matrix K_2 has eigenvalues g_i ($i=1, \dots, m$), then the tensor product of these matrices $K_1 \otimes K_2$ has eigenvalues $s_j \cdot g_i$ [Bellman, 1960]. Figuratively speaking, tensor products of matrices are endowed with the property of "inheritance" of the eigenvalues of these matrices in this form. This property is used in the concept of multi-resonance genetics [Petoukhov, 2016b] and in modeling inherited physiological structures in Mendelian genetics [Petoukhov, 2011, 2021c].

Let us return to the genetic tables of the DNA alphabets of the n -plets in Fig. 1.1, which were built based on binary-oppositional indicators in the alphabet of 4 nucleotides. Using the definition of the tensor product (Fig. A1), one can check that matrices, which are generated by corresponding tensor powers of the matrix [C, A; T, G] of 4 nucleotides (Fig. A2), are identical to the tables of 16 doublets, 64 triplets, 256 tetraplets from Fig. 1.1.

$$\begin{array}{c} \begin{array}{|c|c|} \hline C & A \\ \hline T & G \\ \hline \end{array} \otimes \begin{array}{|c|c|} \hline C & A \\ \hline T & G \\ \hline \end{array} = \begin{array}{|c|c|c|c|} \hline & C & A & \\ \hline C^* & T & G & , A^* \\ \hline & C & A & \\ \hline T^* & T & G & , G^* \\ \hline \end{array} = \begin{array}{|c|c|c|c|} \hline CC & CA & AC & AA \\ \hline CT & CG & AT & AG \\ \hline TC & TA & GC & GA \\ \hline TT & TG & GT & GG \\ \hline \end{array} \\ \\ \begin{array}{|c|c|} \hline C & A \\ \hline T & G \\ \hline \end{array} \otimes \begin{array}{|c|c|} \hline C & A \\ \hline T & G \\ \hline \end{array} \otimes \begin{array}{|c|c|} \hline C & A \\ \hline T & G \\ \hline \end{array} = \begin{array}{|c|c|c|c|c|c|c|c|} \hline CCC & CCA & CAC & CAA & ACC & ACA & AAC & AAA \\ \hline CCT & CCG & CAT & CAG & ACT & ACG & AAT & AAG \\ \hline CTC & CTA & CGC & CGA & ATC & ATA & AGC & AGA \\ \hline CTT & CTG & CGT & CGG & ATT & ATG & AGT & AGG \\ \hline TCC & TCA & TAC & TAA & GCC & GCA & GAC & GAA \\ \hline TCT & TCG & TAT & TAG & GCT & GCG & GAT & GAG \\ \hline TTC & TTA & TGC & TGA & GTC & GTA & GGC & GGA \\ \hline TTT & TTG & TGT & TGG & GTT & GTG & GGT & GGG \\ \hline \end{array} \end{array}$$

Fig. A2. Examples of generating DNA matrices of alphabets of n -plets by exponentiation of the

matrix of four nucleotides [C, A; T, G] to corresponding tensor powers (compare with the tables at Figs. 1.1-1.3).

Acknowledgments

Some results of this paper have been possible due to long-term cooperation between Russian and Hungarian Academies of Sciences on the theme "Non-linear models and symmetrologic analysis in biomechanics, bioinformatics, and the theory of self-organizing systems", where the author was a scientific chief from the Russian Academy of Sciences. The author is grateful to G. Darvas, E. Fimmel, A.A. Koblyakov, M. He, Z.B. Hu, Yu.I. Manin, I.V. Stepanyan, V.I. Svirin, and G.K. Tolokonnikov for their collaboration.

References.

- Abbott D., Davies P.C.W., Pati A.K.** (eds.), Foreword by Sir Roger Penrose. *Quantum Aspects of Life* (2008). ISBN-13: 978-1-84816-253-2
- Alexits G.** *Convergence problems of orthogonal series*. Pergamon (1961).
- Anishchenko V.S., Neiman A.B, Moss F., Shimansky-Geier L.** Stochastic resonance: noise-enhanced order. - *Phys. Usp.*, 42, p. 7–36 (1999). DOI: 10.1070 / PU1999v042n01ABEH000444, <https://ufn.ru/en/articles/1999/1/c/>.
- Astashkin S.** *The Rademacher System in Function Spaces*. Springer Nature Switzerland (2020).
- Bellman R.** *Introduction to Matrix Analysis*. N-Y: McGraw-Hill Book Comp. (1960)].
- Benzi R., Sutera A., Vulpiani A.** The mechanism of stochastic resonance. *Journal of Physics A: Mathematical and General*, 14, 453–457 (1981).
- Benzi R., Sutera A.** Stochastic Resonance in Two Dimensional Landau Ginzburg Equation. *Journal of Physics A General Physics*, July 2004, DOI: 10.1088/0305-4470/37/32/L01, [arXiv:nlin/0308009](https://arxiv.org/abs/nlin/0308009)
- Benzi R.** Stochastic resonance: from climate to biology. - *Nonlin. Processes Geophys.*, 17, 431–441 (2010), www.nonlin-processes-geophys.net/17/431/2010/, doi:10.5194/npg-17-431-2010;
- Berezov T.T., Korovkin B.F.** *Biological chemistry*. Moscow, p. 409 (1990, in Russian).
- Bezrukov S., Vodyanoy I.** Stochastic resonance at the single-cell level. *Nature*, **388**, 633 (1997). <https://doi.org/10.1038/41688>;
- Bodnar O.Ya.** Geometry of phyllotaxis. *Reports of the Academy of Sciences of Ukraine*, №9, pp. 9-15 (1992).
- Bodnar O.Ya.** *Golden Ratio and Non-Euclidean Geometry in Nature and Art*. Lviv: Publishing House "Sweet" (1994).
- Collins J.J., Imhoff T.T., Grigg P.** *Nature*, v.383, p.770 (1996).
- Douglass J.K., Wilkens L., Pantazelou E., Moss F.** *Nature* (London), 365, 337 (1993).
- Dubkov A.A.** *The constructive role of noise in nonlinear nonequilibrium systems*. Nizhny Novgorod State University. N.I. Lobachevsky (2014). <http://www.unn.ru/pages/ranking/method/krshn.pdf>
- Fimmel E., Petoukhov S.V.** Development of Models of Quantum Biology Based on the Tensor Product of Matrices. In: Hu Z., Petoukhov S., He M. (eds). *Advances in Intelligent Systems and Computing*, v. 1126, p.126-135. Springer, Cham (2020), DOI https://doi.org/10.1007/978-3-030-39162-1_12.
- Fimmel E., Strüngmann L.** Yury Borisovich Rumer and his 'biological papers' on the genetic code. – *Phil. Trans. R. Soc. A*, 374: 20150228 (2016). <http://dx.doi.org/10.1098/rsta.2015.0228> .
- Frank-Kamenetskiy M.D.** *The most principal molecule*. Moscow, Nauka (1988) (in Russian).
- Fulton A.B.** *The Cytoskeleton: Cellular Architecture and Choreography*. – Alice Fulton (1984), ISBN 0412255103, 9780412255106.
- Gerber R.** *Vibrational Medicine: New Choices for Healing Ourselves*. Bear & Co, 1996
- Gilyarov M.S.** *Biological Encyclopedic Dictionary*. Moscow: Sov. Encyclopedia (1989) (in Russian).
- Gold B., Rader C. M.** *Digital Processing of Signals*. McGraw–Hill: New York, USA (1969).

- Gurvich A.G.** *Selected Works*. Moscow: Medicine (1977).
- Hu Z.B., Petoukhov S.V., Petukhova E.S.** I-Ching, dyadic groups of binary numbers and the geno-logic coding in living bodies. *Progress in Biophysics and Molecular Biology*, vol. 131, pp. 354-368 (December 2017).
- Igamberdiev A.U.** Quantum mechanical properties of biosystems: a framework for complexity, structural stability, and transformations. *Biosystems*, 31(1), p. 65–73 (1993).
- Jordan P.** Die Quantenmechanik und die Grundprobleme der Biologie und Psychologie. (Quantum mechanics and the fundamental problems of biology and psychology). *Naturwissenschaften* 20, 815–821 (1932), DOI:10.1007/BF01494844.
- Kac M.** *Statistical independence in probability, analysis and number theory*. Math. Assoc. Amer. (1959).
- Kaczmarz S., Steinhaus H.** *Theorie der Orthogonalreihen*, Chelsea, reprint (1951);
- Karp A.H.** Bit reversal on uniprocessors. *SIAM Review*, v. 38 (1), p.1–26 (1996), doi:[10.1137/1038001](https://doi.org/10.1137/1038001), MR [1379039](https://www.jstor.org/stable/2386399).
- Karzel H., Kist G.** Kinematic Algebras and their Geometries, in *Rings and Geometry*, R. Kaya, P. Plaumann, and K. Strambach editors, p. 437–509, esp 449,50, D. Reidel (1985). ISBN 90-277-2112-2.
- Kienle G.** Experiments concerning the non-Euclidean structure of visual space. In *Bioastronautics*. Pergamon Press: New York, NY, USA, 1964; pp. 386–400.
- Krauss P., Tziridis K., Achim Schilling A., Schulze H.** Cross-Modal Stochastic Resonance as a Universal Principle to Enhance Sensory Processing. - *Frontiers in Neuroscience* , Volume 12 | Article 578 (1 August 2018). doi: 10.3389/fnins.2018.00578, <https://www.frontiersin.org/articles/10.3389/fnins.2018.00578/full>
- Levin J.E., Miller J.P.** *Nature* (London), 380, 165 (1996).
- Lin Cui, Junan Yang, Lunwen Wang, Hui Liu.** Adaptive Unsaturated Bistable Stochastic Resonance Multi-Frequency Signals Detection Based on Preprocessing. *Electronics*, 10, 2055 (2021). <https://doi.org/10.3390/electronics10172055>).
- Longtin A.** *J. Stat. Phys.* V.70, P.309 (1993).
- Lyons R.** Understanding Digital Signal Processing. Pearson; 3rd edition, 954 pages, (2010), ISBN-10: 0137027419, ISBN-13: 978-0137027415.
- Matsuno K.** Cell motility as entangled quantum coherence. *BioSystems*, 51, p. 15–19 (1999).
- Matsuno K., Paton R.C.** Is there a biology of quantum information? *BioSystems*, 55, p. 39–46 (2000).
- McFadden J., Al-Khalili J.** The origins of quantum biology. *Proceedings of the Royal Society A*, Vol. 474, Issue 2220, p. 1-13, 12 December 2018, <https://doi.org/10.1098/rspa.2018.0674>.
- Moss F.** Stochastic Resonance at the Molecular Level. *Biophysical Journal*, v. 73, November 1997, p. 2249-2250.
- Nicolis C.** Stochastic aspects of climatic transitions—response to a periodic forcing, *Tellus*, 34:1, 1-9 (1982). DOI: 10.3402/tellusa.v34i1.10781
- Nielsen M.A., Chuang I.L.** *Quantum Computation and Quantum Information*. New York: Cambridge University Press. <https://doi.org/10.1017/CBO9780511976667> (2010).
- Pastawski F., Yoshida B., Harlow D., Preskill J.** Holographic quantum error-correcting codes: toy models for the bulk/boundary correspondence. *J. High Energy Phys.*, 149 (2015). [https://doi.org/10.1007/JHEP06\(2015\)149](https://doi.org/10.1007/JHEP06(2015)149), <https://link.springer.com/article/10.1007%2FJHEP06%282015%29149#citeas>.
- Patel A.** Quantum algorithms and the genetic code. *Pramana – J. Phys.* 56(2–3), p. 367–381, arXiv:quant-ph/0002037 (2001a).
- Patel A.** Testing quantum dynamics in genetic information processing. *J. Genet.* 80(1), p. 39–43 (2001b).
- Patel A.** Why genetic information processing could have a quantum basis. *J. Biosci.* 26(2), p. 145–151 (2001c).
- Pei X., Wilkens L., Moss F.** *J. Neurophysiol.* 76, 3002 (1996).
- Petoukhov S.V.** Non-Euclidean geometries and algorithms of living bodies. *Computers and Mathematics with Applications*, v. 17, № 4-6, p. 505-534 (1989). <http://petoukhov.com/petoukhov-symmetry-2-geometry.pdf> .
- Petoukhov S.V.** Genetic Codes II: Numeric rules of degeneracy and a chronocyclic theory. – *Symmetry*

in *Genetic Information*, ed. Petoukhov S.V. (2001), ISBN 963216 242 0, special double issue of the journal “Symmetry: Culture and Science”, Budapest: International Symmetry Foundation, v.12, #3-4, pp. 275-306 (2001).

http://petoukhov.com/GENETIC_CODE_AND_CHRONOCYCLIC_APPROACH_2001_PETOUKHOV.pdf

Petoukhov S.V. The rules of degeneracy and segregations in genetic codes. The chronocyclic conception and parallels with Mendel’s laws. – “Advances in Bioinformatics and its Applications” (editors – M.He, G.Narasimhan, S.Petoukhov), Proceedings of the International Conference (Florida, USA, 16-19 December 2004), Series in Mathematical Biology and Medicine, v.8, pp.512-532 (2005), New Jersey–London–Singapore–Beijing, World Scientific, ISBN 981-256-148-X.

http://petoukhov.com/CHRONOCYCLIC_CONCEPT_AND_DEGENERACY_OF_GENETIC_CODE_2005_PETOUKHOV.pdf

Petoukhov S.V. *Matrix genetics, algebraic bases of genetic code, noise immunity*. Moscow, RCD, 316 p. (2008a, in Russian). ISBN 978-5-93972-643-6. <http://petoukhov.com/matrix-genetics-petoukhov-2008.pdf>

Petoukhov S.V. Matrix genetics and algebraic properties of the multi-level system of genetic alphabets. *Neuroquantology*, v. 9, №4, p. 60-81 (2011).

http://petoukhov.com/NEUROQUANTOLOGY_PAPER_PETOUKHOV_2011.pdf

Petoukhov S.V. The genetic code, 8-dimensional hypercomplex numbers and dyadic shifts. – <http://arxiv.org/abs/1102.3596>, 11th version (15 July 2016a).

Petoukhov S.V. The system-resonance approach in modeling genetic structures. *Biosystems*, v. 139, p. 1-11 (January 2016b).

Petoukhov S.V. The Genetic Code, 8-Dimensional Hypercomplex Numbers and Dyadic Shifts. 11th Version of the Article. Available online: <http://arxiv.org/abs/1102.3596> (15 July 2016c).

Petoukhov S.V. The Genetic Coding System and Unitary Matrices. *Preprints* 2018, 2018040131 (2018), doi: 10.20944/preprints201804.0131.v2.

Petoukhov S.V. Nucleotide Epi-Chains and New Nucleotide Probability Rules in Long DNA Sequences. *Preprints* 2019, 2019040011, version 2, 41 pages (2019a) (doi: 10.20944/preprints201904.0011.v2), <https://www.preprints.org/manuscript/201904.0011/v2>

Petoukhov S. Hyperbolic Numbers in Modeling Genetic Phenomena. *Preprints* 2019, 2019080284 (2019b). DOI: 10.20944/preprints201908.0284.v4.

Petoukhov S.V. Hyperbolic Rules of the Cooperative Organization of Eukaryotic and Prokaryotic Genomes. *Biosystems*, 198, 104273 (2020a).

Petoukhov S.V. Hyperbolic Rules of the Oligomer Cooperative Organization of Eukaryotic and Prokaryotic Genomes. *Preprints* 2020, 2020050471 (2020b), doi:10.20944/preprints202005.0471.v2, <https://www.preprints.org/manuscript/202005.0471/v2>.

Petoukhov S.V. The rules of long DNA-sequences and tetra-groups of oligonucleotides. [arXiv:1709.04943v6](https://arxiv.org/abs/1709.04943v6), 174 pages, 6th version from 22.05.2020 (2020c).

Petoukhov S.V. Algebraic harmony and probabilities in genomes. Long-range coherence in quantum code biology. – *Biosystems*, v. 209, 104503 (November 2021a). Available online 20 August 2021, 104503, <https://doi.org/10.1016/j.biosystems.2021.104503>.

Petoukhov S.V. Algebraic Rules for the Percentage Composition of Oligomers in Genomes. *Preprints* 2021, 2021010360, 3rd version, 84 pages (2021b). DOI: 10.20944/preprints202101.0360.v3. <https://www.preprints.org/manuscript/202101.0360/v3>.

Petoukhov S.V. Modeling inherited physiological structures based on hyperbolic numbers, *BioSystems*, Vol. 199, 104285 (2021c), ISSN 0303-2647, <https://doi.org/10.1016/j.biosystems.2020.104285>.

Petoukhov S.V., He M. *Symmetrical Analysis Techniques for Genetic Systems and Bioinformatics: Advanced Patterns and Applications*. Hershey, USA, IGI Global (2010). <http://petoukhov.com/Petoukhov,%20He%20-%20202010%20-%20Symmetrical%20Analysis%20Techniques%20for%20Genetic%20Systems%20and%20Bioinformatics.pdf>

Petoukhov S.V., Petukhova E.S., Svirin V.I. Symmetries of DNA alphabets and quantum informational formalisms. *Symmetry: Culture and Science*, Vol. 30, No. 2, p.161-179 (2019), https://doi.org/10.26830/symmetry_2019_2_161.

Prabhu V. V. Symmetry observation in long nucleotide sequences. *Nucleic Acids Res.*, 21, 2797-2800 (1993).

